Designing large-eddy simulation of the turbulent boundary layer to capture law-of-the-wall scaling[a)]

James G. Brasseur and Tie Wei

Citation: Physics of Fluids **22**, 021303 (2010); doi: 10.1063/1.3319073
View online: http://dx.doi.org/10.1063/1.3319073
View Table of Contents: http://scitation.aip.org/content/aip/journal/pof2/22/2?ver=pdfcov
Published by the AIP Publishing

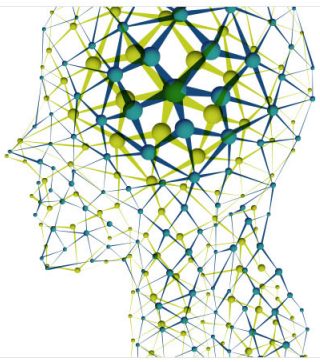

Designing large-eddy simulation of the turbulent boundary layer to capture law-of-the-wall scaling[a)]

James G. Brasseur[b)] and Tie Wei (韦铁)
Department of Mechanical Engineering, The Pennsylvania State University, University Park, Pennsylvania 16802, USA

(Received 18 September 2009; accepted 5 January 2010; published online 25 February 2010)

Law-of-the-wall (LOTW) scaling implies that at sufficiently high Reynolds numbers the mean velocity gradient $\partial U/\partial z$ in the turbulent boundary layer should scale on u_*/z in the inertia-dominated surface layer, where u_* is the friction velocity and z is the distance from the surface. In 1992, Mason and Thomson pointed out that large-eddy simulation (LES) of the atmospheric boundary layer (ABL) creates a systematic peak in $\phi(z) \equiv (\partial U/\partial z)/(u_*/z)$ in the surface layer. This "overshoot" is particularly evident when the first grid level is within the inertial surface layer and in hybrid LES/Reynolds-averaged Navier–Stokes methods such as "detached-eddy simulation," where the overshoot is identified as a "logarithmic layer mismatch." Negative consequences of the overshoot—spurious streamwise coherence, large-eddy structure, and vertical transport—are enhanced by buoyancy. Several studies have shown that adjustments to the modeling of the subfilter scale (SFS) stress tensor can alter the degree of the overshoot. A comparison among simulations indicates a lack of grid independence in the prediction of mean velocity that originates in surface layer deviations from LOTW. Here we analyze the broader framework of LES prediction of LOTW scaling—including, but extending beyond, "the overshoot." Our theory includes a criterion that is necessary to remove the overshoot but is insufficient for LES to produce constant $\phi(z) \equiv 1/\kappa$ through the surface layer, and fully satisfy the LOTW. For mean shear to scale on u_*/z in the surface layer, we show that two additional criteria must be satisfied. These criteria can be framed in terms of three nondimensional variables that define a parameter space in which systematic adjustments can be made to the simulation to achieve LOTW scaling. This occurs when the three parameters exceed critical values that we estimate from basic scaling arguments. The essential difficulty can be traced to a spurious numerical LES viscous length scale that interferes with the dimensional analysis underlying LOTW. When this spurious scale is suppressed sufficiently to retrieve LOTW scaling, the LES has been moved into the supercritical "high accuracy zone" (HAZ) of our parameter space. Using eddy viscosity closures for SFS stress, we show that to move the simulation into the HAZ, the model constant must be adjusted together with grid aspect ratio in coordinated fashion while guaranteeing that the surface layer is sufficiently well resolved in the vertical by the grid. We argue that, in principle, both the critical values that define the HAZ and the surface layer constant κ when LOTW scaling is achieved can depend on details of the SFS (and surface stress) models applied in the LES. We carried out over 110 simulations of the neutral rough-surface ABL to cover a wide portion of the parameter space using a low dissipation spectral code, the Smagorinsky SFS stress model and a standard model for fluctuating surface stress. The overshoot was found to systematically reduce and $\phi(z)$ was found to systematically approach a constant value in the surface layer as the three parameters exceeded critical values and the LES moved into the HAZ, consistent with the theory. However, whereas constant $\phi(z)$ was achieved over nearly the entire surface layer as the LES is moved into the HAZ, the model for surface shear stress continues to disrupt LOTW scaling at the first couple grid levels, and the predicted von Kármán constant κ is lower than traditional values. In a comprehensive discussion, we summarize the primary results of subsequent studies where we minimize the spurious influence of the surface stress model and show that the surface stress model and the SFS stress model constant influence the predicted value of the von Kármán constant for LES in the HAZ. © *2010 American Institute of Physics*. [doi:10.1063/1.3319073]

[a)]This paper is based on an invited lecture, which was presented by the first author at the 61st Annual Meeting of the Division of Fluid Dynamics of the American Physical Society, held 23–25 November 2008 in San Antonio, TX.

[b)]Author to whom correspondence should be addressed. Electronic mail: brasseur@psu.edu. Telephone: +1 (814) 865-3159.

I. INTRODUCTION

Accurate prediction of mean velocity and mean velocity gradient are prerequisites to large-eddy simulation (LES) predictions of wall-bounded shear flows at the highest levels of accuracy within the constraints of LES. Mean velocity gradient, in particular, enters the Reynolds stress as a source in streamwise velocity variance and affects directly the large-eddy structure and corresponding turbulent transport. We ask what basic characteristics of a subfilter scale (SFS) stress model together with the grid and the numerical algorithm are required for a LES to capture the law-of-the-wall (LOTW) in the inertia-dominated surface layer with the least alteration to the true Navier–Stokes physics. Alterations could include, for example, the addition of numerical dissipation or algorithmic modifications made in the computational domain or at its boundaries to force a logarithmic mean velocity profile to exist.

At its root, LOTW follows from scaling arguments with the assumption that at sufficiently high outer Reynolds numbers, only one characteristic length and velocity scale are relevant to the vertical gradient of mean velocity, $\partial U/\partial z$, within a "surface layer" adjacent to a flat solid boundary that is directly influenced by surface blockage (U is the mean horizontal velocity magnitude and z is the vertical coordinate from the surface). If the surface is aerodynamically smooth, LOTW assumes the existence of a viscous surface layer directly adjacent to the surface that is characterized by the single length scale $\ell_\nu = \nu/u_*$, where ρu_*^2 is the mean surface shear stress and ν is the fluid kinematic viscosity. If the surface is homogeneously rough, the characteristic roughness scale z_0 must enter the scaling immediately adjacent to the surface. Under LOTW, an inertial surface layer is assumed to exist outside the viscous surface layer that is sufficiently far from the surface that neither ℓ_ν nor z_0 are relevant scales and that the only length scale relevant to $\partial U/\partial z$ is the distance from the surface z, characterizing a dominant integral scale of underlying turbulence fluctuations. LOTW assumes that u_* is the only characteristic velocity scale across the entire surface layer, so that the transition between ℓ_ν and z as dominant length scales is the primary distinction between the viscous and inertial surface layers. Consequently, according to LOTW $\partial U/\partial z \sim u_*/\ell_\nu$ in the viscous surface layer and $\partial U/\partial z \sim u_*/z$ in the inertial surface layer. If any other length or velocity scales significantly affect the mean velocity field, these scales will disrupt the LOTW scalings for $\partial U/\partial z$.

We consider a boundary layer where the Reynolds number is so high that the viscous layer is unresolvable in the vertical, or that roughness elements have a scale well below the vertical dimension of the first grid cell adjacent to the surface, that is $\ell_\nu \ll \Delta_z$ and/or $z_0 \ll \Delta_z$, where Δ_z is the vertical grid size (assuming a uniform grid). Thus, neither ℓ_ν nor z_0 enter the boundary layer dynamics and scalings that are resolved on the grid and the viscous force term in the resolved Navier–Stokes equation is negligible; viscous dissipation occurs at scales far below the grid and viscous effects enter only indirectly through the inertial transfer of momentum and energy between resolved and SFS motions.

In 1992, Mason and Thomson[1] pointed out a fundamental flaw in LES predictions of high Reynolds number turbulent boundary layers: the mean velocity gradient scaled according to inertial LOTW scaling produces a well-defined peak within the surface layer; the LES does not predict the LOTW. This "overshoot" has since been pointed out and studied by many researchers. In Fig. 1 we show several examples of the overshoot from the literature, where the vertical gradient of mean streamwise velocity is plotted normalized by inertial LOTW surface-layer velocity and length scales

$$\phi(z) \equiv \frac{z}{u_*}\frac{\partial U}{\partial z}. \tag{1}$$

In Fig. 1 $\Phi_m(z) \equiv \kappa\phi(z)$ is plotted against z, where κ is the von Kármán constant, assumed to be 0.4. LOTW scaling implies that $\phi(z)$ should be constant through the inertial surface layer, the lower 15%–20% of the boundary layer depth. Estimation of the value κ that makes $\Phi_m = 1$ through the surface layer in the high Reynolds number limit is difficult from laboratory experiment, in part because the high Reynolds number limit is difficult to know, u_* is difficult to measure accurately, and pressure and other corrections are sometimes applied to the data. In the atmospheric boundary layer (ABL) where Reynolds number is not a major concern, global stability and lack of stationarity are. Recent compilations of experimental data by Nagib and Chauhan[6] conclude that "the von Kármán coefficient is not universal and exhibits dependence on not only the pressure gradient but also on the flow geometry…" They estimate κ over the range from ≈ 0.37 in channel flow to ≈ 0.41 in pipe flow, with a flat plate boundary layer estimate in between at $\kappa \approx 0.384$. In the near-neutral rough ABL Andreas *et al.*[7] recently estimated $\kappa \approx 0.387$; however, they quote experimental values from the literature as low as 0.33 (Ref. 8) and as high as 0.40 (Ref. 9) with several studies reporting κ in the range of 0.35–0.37.[10–13]

In Fig. 1 Φ_m is plotted against z nondimensionalized by a boundary layer depth or, in Fig. 1(b), by a Coriolis scale. The overshoot shows up clearly in many of these plots as a peak in Φ_m in the surface layer, highlighted in gray. Figure 1 indicates that the overshoot is the most obvious manifestation of a broader problem—the apparent inability for LES to predict LOTW scaling within the high Reynolds number turbulent surface layer. Similarly, a near-surface overshoot has also been observed in the mean gradient of temperature.[2,14]

Methods to reduce or eliminate the degree of overshoot have universally centered on modifying the closure for the SFS stress tensor (e.g., Fig. 1); however, these have been developed in the absence of a clear understanding of itssource. In this study we develop a theory to explain the fundamental characteristics underlying both the overshoot and the inability for LES to capture scaling for mean velocity gradient consistent with LOTW in the inertial surface layer— that is, constant $\phi(z)$ through the lower 15%–20% of the boundary layer. From this theory we develop requirements for the LES to predict LOTW scaling that integrate the design of basic features of the SFS stress model with the design of the simulation, particularly the grid. We further show that it is

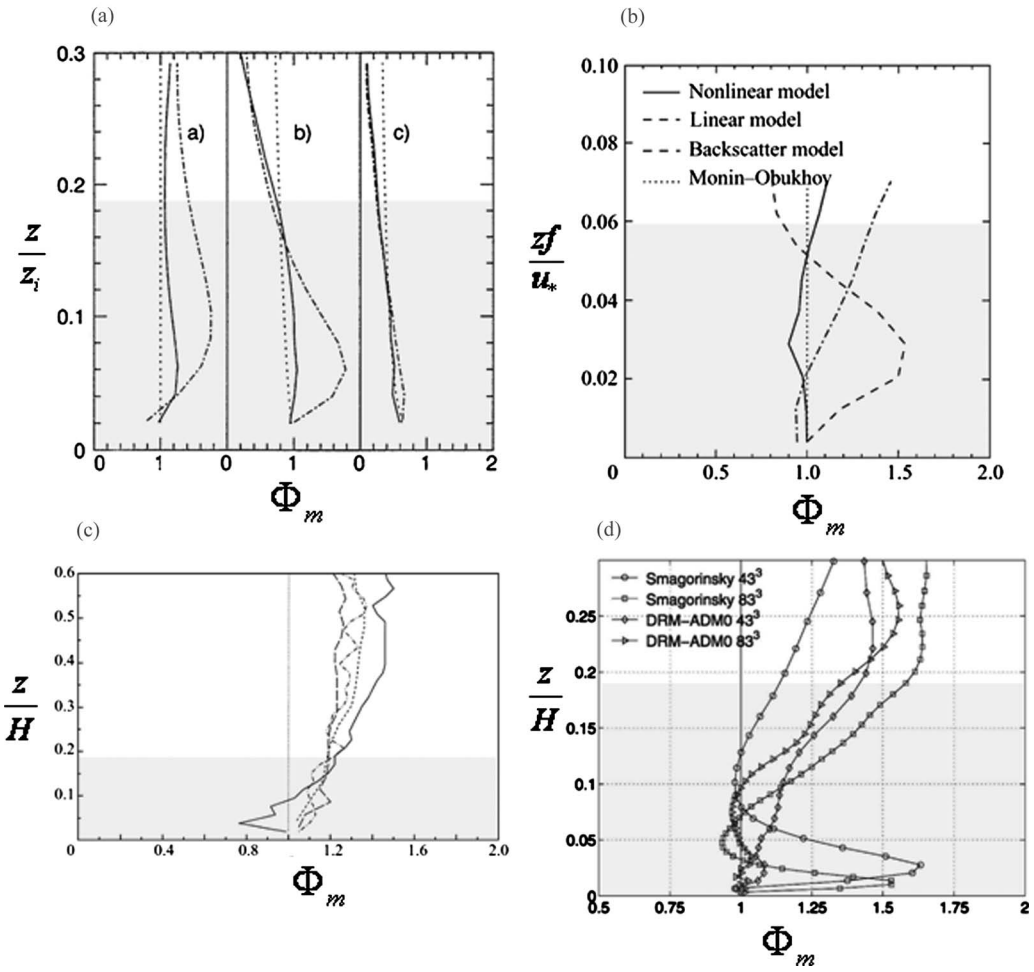

FIG. 1. Examples of the overshoot in mean shear from previous LES studies: (a) Sullivan *et al.* (Ref. 2), (b) Kosovic (Ref. 3), (c) Porté-Agel *et al.* (Ref. 4), and (d) Chow *et al.* (Ref. 5). In (a) z_i is the ABL depth defined in the traditional manner as the height where vertical turbulent heat flux is a minimum. In (b) z is scaled on u_*/f, where f is the Coriolis parameter (the angular velocity at the earth's surface). The simulations in (c) and (d) are pseudo-ABL/channel flow simulations which do not contain a capping inversion and instead apply fixed horizontal velocity at $z=H$. $\kappa=0.4$ was assumed in forming Φ_m. The shaded regions indicate the surface layer.

possible to eliminate the overshoot without the LES predicting LOTW scaling; eliminating the overshoot is a necessary but not a sufficient condition to predict LOTW. From the theory we design a three-variable parameter space in which the SFS model parameters and LES grid can be adjusted to systematically weaken the influence of a spurious "numerical LES viscous length scale" until the LES predicts LOTW scaling in the surface layer. Although the basic theory is independent of any particular SFS stress closure, we use eddy viscosity models to gain insight into the theory and to develop a practical approach to designing LES within the parameter space.

We then present numerical experiments to show that the theory accounts for primary characteristics underlying LOTW scaling with LES. However we also learn that when LOTW scaling is achieved, two previously hidden issues appear: the surface shear stress model interferes with LOTW scaling at the first couple grid levels, and both the surface stress model and an interaction between SFS stress model and aspect ratio influence the predicted value of the $\phi \equiv 1/\kappa$ in the surface layer when constant $\phi(z)$ is achieved. We discuss these two issues broadly within the "Discussion," Sec. VII.

The framework we present here has broader implications to the transition between LES and Reynolds-averaged Navier–Stokes (RANS) calculations,[15] and to the interplay among modeling, grid, and algorithm. In particular, our analysis is relevant to hybrid LES-RANS approaches such as "detached-eddy simulation"[16] (DES), where the overshoot is identified as a "log-layer mismatch" or "superbuffer layer."[17–19] We discuss the applicability of the current study in Secs. II B and VII D.

II. BACKGROUND ON "THE OVERSHOOT PROBLEM"

Before developing our analysis into essential mechanisms underlying LES prediction of LOTW scaling of mean velocity gradient, we set the stage with a discussion of the overshoot and its history. Previous studies, many of which have produced significant reductions in the degree of overshoot, provided important clues that lead to the theory developed here, and present results that a theory should explain.

A. Consequences of an overshoot in mean shear rate

Figure 1 shows the essential aspects of the overshoot from several previous LESs of the neutral boundary layer that have focused on this issue since Mason and Thomson.[1] Because the overshoot is associated with the shear-dominated region of the boundary layer, it is particularly apparent in the fully shear-driven neutral boundary layer (Fig. 1). Piomelli and Balaras[19] point out that in DES of the shear-driven boundary layer, "unphysical, nearly one-dimensional wall streaks were present in the RANS region…and shorter-scale outer-layer eddies were progressively formed as one moved away from the wall." Similar observations have been made in the neutral ABL.[20]

In the moderately convective ABL an overshoot is produced in the shear-dominated surface layer while the mixed layer is buoyancy dominated.[21] In the presence of convection, vertically driven thermals couple the surface and outer boundary layers. Khanna and Brasseur[20] showed that the elongated structure of streamwise turbulence fluctuations generated near the surface by the interaction between strong mean shear and turbulence (streaks) is the source of thermals that penetrate the outer boundary layer. These coherent elongated vertical motions interact with the horizontal mean wind to form highly coherent secondary rolls that extend to the top of the boundary layer and can extend 20–40 boundary layer thicknesses in the mean wind direction.[22] Thus, there is a direct coupling between the near-surface shear-driven streaks and very large eddy structure of the boundary layer. (It is possible that the mechanisms that underlie the creation of the longitudinal convective rolls may be related to the mechanisms underlying much weaker highly elongated structures that have been observed in the log layer of the neutral boundary layer.[23])

An important negative consequence of the inner-outer coupling is that the near-surface errors from the overshoot are driven vertically to infect the entire boundary layer. To demonstrate this, Khanna and Brasseur[20] applied two SFS models to the same LES; one produced a stronger overshoot than the other. The LES with the stronger overshoot produced much stronger and coherent convective thermals and boundary layer rolls with much larger horizontal integral scales that persisted to the top of the boundary layer. Furthermore, these overly coherent thermals are spuriously aligned with the mean geostrophic wind. This spuriously strong thermal structure adversely influences vertical transport to the upper atmosphere of momentum, thermal energy, contaminants, and humidity. Error in humidity predictions will likely enter cloud cover predictions and produce error in solar radiative heating at the earth's surface. Incorrect prediction of vertical transport of CO_2 and other greenhouse gases may affect related predictions of upper atmosphere chemistry.

The negative consequences of the overshoot in mean velocity gradient arise essentially from the incorrect prediction of Reynolds stress anisotropy near the surface. Juneja and Brasseur[24] argued that the incorrect anisotropy results from a feedback interaction between the exaggerated mean gradient and Reynolds stress production as a consequence of inherent under-resolution at the first grid level that occurs in LES of high Reynolds number turbulent boundary layers when the first grid level is in the inertial layer. The errors are exacerbated by any mechanism that enhances vertical transport, including buoyancy[20] and boundary layer separation.

B. Previous studies

Given the importance of the overshoot, there have been a number of studies that have attempted either to understand the cause of the overshoot,[24] or have attempted to remove it. Mason and Thomson,[1] for example, suggested that the overshoot is particular to eddy viscosity closures where energy is removed at each point from the resolved scales in contrast with the known forward/backward nature of energy transfer at a point. To introduce "backscatter" into the simulation, they added to the resolved momentum equation a Langevin-like stochastic acceleration term, in addition to a SFS stress divergence using the Smagorinsky closure for SFS stress. However, Mason and Thomson[1] made another significant modification—they reduced the eddy viscosity near the surface by making the Smagorinsky length scale proportional to z at grid nodes near the surface.

In Fig. 1 we compare the results from four other groups of researchers between 1994 and 2005 who explicitly addressed the problem of the overshoot in LES of the ABL. The surface layer is shaded to indicate the region over which Φ_m should be predicted as a straight vertical line and from which a grid-independent prediction for mean velocity should emanate. Figure 1(a) shows predictions from Sullivan *et al.*[2] who argued that as the surface is approached, the SFS stress closure should transition from an eddy viscosity model appropriate to LES to a model more appropriate to the RANS equation. Although their mixed eddy viscosity model was purely dissipative (no backscatter), the overshoot was significantly reduced compared with a pure SFS model. Like Mason and Thomson,[1] their mixed model results in a reduction in net SFS stress and eddy viscosity near the surface. Whereas the overshoot could be reduced, and perhaps even eliminated, by the adjustments to the SFS model, a dependence of $\phi(z)$ on z persisted [Fig. 1(a)]. The Sullivan *et al.*[2] model was further modified by Ding *et al.*[25] Recently, Lévêque *et al.*[26] modified the Smagorinsky eddy viscosity by subtracting mean shear from the instantaneous resolved rate-of-strain tensor. Whereas they applied the model only to low Reynolds number boundary layers with partially resolved viscous layers, the effect is again to reduce the eddy viscosity near the surface. However the LES predictions failed to predict constant $\phi(z)$ over the entire surface layer.

Kosovic[3] added additional nonlinear terms in velocity gradient to the eddy viscosity closure. Whereas a major improvement in the overshoot in the neutral ABL was obtained [Fig. 1(b)], grid resolution was quite low and the improvement degraded at higher grid resolution. Dynamic formulations of the Smagorinsky eddy viscosity closure have been applied by Porté-Agel *et al.*[4] and Esau[27] to improve the overshoot and capture the LOTW. We show in Fig. 1(c) the results from Porté-Agel *et al.*[4] who developed a scale-dependent formulation of the dynamic Smagorinsky model

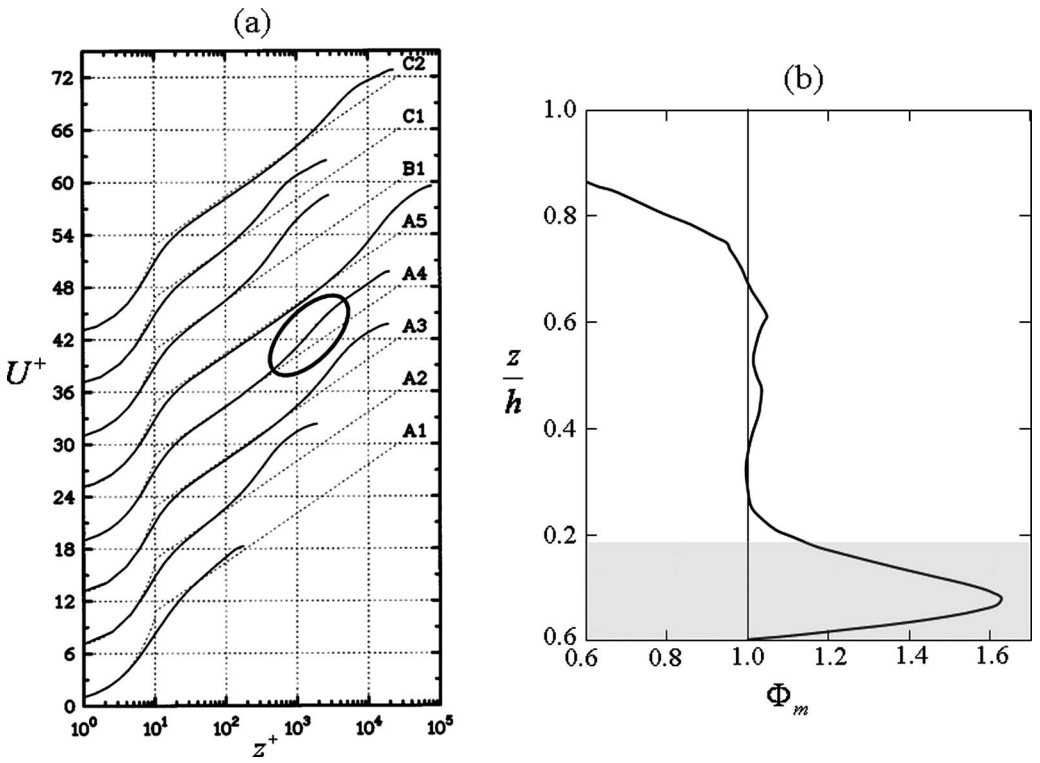

FIG. 2. The logarithmic layer mismatch in the smooth wall turbulent channel flow DESs of Nikitin *et al.* (Ref. 17) discussed by Spalart (Ref. 18). Curve A4 is the simulation in (b); Re_τ=20 000. (a) $U^+=U/u^*$ plotted against $z^+=z/\ell_\nu$. (b) The "log layer mismatch" shown by the upper oval in (a) is shown here to be an overshoot in normalized mean shear Φ_m, negating LOTW scaling over the surface layer (shaded area). (b) was kindly generated by Spalart (Ref. 33). κ is assumed to be 0.4.

that produces a reduction in eddy viscosity near the surface and removes an apparent undershoot with the standard dynamic model (solid line). Whereas the modifications significantly reduced the overshoot, constant $\phi(z)$ was not obtained over the surface layer.

Chow *et al.*[5] combined a number of modeling elements, including a dynamic eddy viscosity model,[28] a "resolvable SFS stress model" component[29] combined with a deconvolution procedure,[30] and a "canopy model."[31] As shown in Fig. 1(d), whereas overprediction of mean shear near the surface could be reduced with certain combinations of elements, it was not clear which modeling elements were responsible, and a robust grid-independent solution was not obtained. A recent calculation by Drobinski *et al.*,[32] however, indicated that a suppression of the overshoot was possible using a standard one-equation model but with a more refined grid. Their result will be discussed in Secs. VI B and VII B in context with the current analysis.

Figure 2 shows that what we refer to here as an overshoot is described as a "logarithmic layer mismatch" or superbuffer layer in the DESs of Nikitin *et al.*[17] Spalart[18] and Piomelli and Balaras[19] described this as a fundamental unresolved problem in DES. Whereas the simulations of Fig. 1 contain only the inertial LOTW layer due to the presence of surface roughness and the fluctuating surface stress is modeled, the DES uses RANS to model a viscous surface layer with no slip at the wall [shown in Fig. 2(a)] below an inertial-dominated surface layer that is simulated with LES, as shown in Fig. 2(b). The logarithmic layer mismatch, shown by the circled part of the mean velocity profile, Fig. 2(a), is shown in Fig. 2(b) to be equivalent to the overshoot phenomenon discussed above.

Figures 1 and 2 motivate the current research; we seek an understanding of the essential mechanisms underlying the overshoot and, from that, a method that will both eliminate the overshoot and predict a vertical line in Φ_m versus z over the entire surface layer with a grid-independent prediction over the entire boundary layer. Historically, the assumption has been that the solution to the overshoot problem is a closure issue, and all attempts to modify LES to predict LOTW have been through adjustments to the SFS stress tensor model. Although there have been significant advances made, the fundamental mechanisms underlying the overshoot are not understood so that a clear path to robust grid-independent LES that eliminates the overshoot and predicts LOTW scaling has been elusive. We show here that the fundamental issues underlying the overshoot and its resolution are broader than the SFS model and involve the basic characteristics of the SFS stress closure integrated with the construction of the LES grid.

C. Useful clues

In the studies described above, a number of important observations have been made that provide clues to underlying issues and which require explanation:

(1) The overshoot is influenced by the details of the SFS model. This has been discussed above in Sec. II B (Fig.

1). Whereas there have been many variants to the modeling process, all have employed an eddy viscosity component. A common characteristic of the more successful adjustments to the modeling process is a reduction in eddy viscosity near the surface, as compared with unadulterated models.

(2) The overshoot is tied to the grid. Khanna and Brasseur[21] pointed out that increasing the resolution of the grid, keeping all other elements of the simulation unchanged, does not diminish the magnitude of the overshoot, but moves the peak in Φ_m closer to the surface in proportion to the vertical grid spacing, Δ_z. Similarly, Spalart[18] pointed out that in DES "grid refinement merely moves the same amount of (logarithmic layer) mismatch closer to the wall." This dependence of the overshoot on grid resolution is clear, for example, in Fig. 1(d). Why the location of the overshoot should be proportional to Δ_z, however, is not understood. Khanna and Brasseur[21] pointed out that because the horizontal integral scale of vertical velocity scales on z, vertical velocity is always under-resolved at the first grid level independent of grid resolution and that this under-resolution has negative consequences that must be addressed to eliminate the overshoot. Specifically, they proposed that this inherent under-resolution at the first grid level somehow ties the overshoot to the grid. The mechanisms were unclear, but were felt to be somehow associated with the lack of performance of SFS models when the integral scales are under-resolved. This shall be discussed in Sec. IV B

(3) The prediction of mean velocity gradient is grid dependent. A requirement for any successful numerical simulation is grid independence in the solution for mean variables.[34] As illustrated in Fig. 1(d), the solution for mean velocity gradient often does not converge as the grid is refined; each grid produces a different solution not only in the overshoot region but throughout the boundary layer. Grid dependence in the flow is apparent when different solutions in the literature are compared (e.g., Andren *et al.*[14]). We shall show in Sec. VI B that a grid-independent solution is only possible when both the overshoot is suppressed and LOTW scaling is obtained.

It is apparent from these previous studies that although the overshoot is influenced by the closure for SFS stress, the overshoot problem is only part of the broader issue of accurately predicting the LOTW, and that these are both modeling and numerical issues.

III. AN ANALYSIS OF THE FUNDAMENTAL NATURE OF THE OVERSHOOT: THE FIRST OBSERVATION

In this section we focus specifically on the overshoot. A primary mechanism underlying the overshoot and its resolution can be understood by comparing true inertial-versus-viscous scaling underlying the stationary fully developed smooth wall channel flow in the high Reynolds number limit with scaling of LES of the same high Reynolds number channel flow with an unresolved viscous or roughness layer. We shall find that we can relate the true physics of the channel flow to the spurious physics of the simulated channel flow that is model and algorithmically dependent and cannot be entirely eliminated.

A. Scaling high Reynolds number smooth wall turbulent channel flow

Consider a fully developed stationary smooth wall incompressible channel flow at Reynolds numbers sufficiently high to support the classical LOTW in the surface layer. The local and global mean axial momentum balances are, respectively,

$$\frac{\partial P}{\partial x} = \frac{\partial T_t(z)}{\partial z} + \frac{\partial T_\nu(z)}{\partial z} = \frac{\partial T_{\rm tot}(z)}{\partial z} \quad \text{and} \quad \frac{\partial P}{\partial x} = -\frac{T_0}{\delta}, \tag{2}$$

where $T_0 \equiv T_{\rm tot}(0) \equiv \rho u_*^2$ and δ is the half channel width or boundary layer depth (the height where $T_{\rm tot}=0$). The second expression in Eq. (2) results from a global force balance. The coordinates (x,y,z) are in the mean-flow, spanwise, and wall-normal directions, respectively. $P(x)$ is the mean pressure and $T_{\rm tot}=T_t+T_\nu$ is the total mean stress, where T_t and T_ν are Reynolds stress and mean viscous stress, respectively,

$$T_t(z) = -\rho\langle u'w'\rangle, \quad T_\nu(z) = \mu\frac{\partial U}{\partial z}. \tag{3}$$

Capital letters and primed quantities indicate mean flow and fluctuating variables, respectively, (u,v,w) are the velocity components in the (x,y,z) directions, (ρ,μ) are density and viscosity, and the angle brackets denote ensemble averaging.

Integrating Eq. (2) in z and replacing $T_\nu(z)$ with $(\mu u_*/\kappa z)\Phi_m(z)$, the exact equation for the normalized mean gradient is

$$\Phi_m(z) = \kappa z^+\left(1 - T_t^+(z) - \frac{z}{\delta}\right), \tag{4}$$

where $T_t^+ = T_t/T_0$ is the ratio of the Reynolds stress $T_t(z)$ to the wall stress T_0, and $z^+ = z/\ell_\nu$ is the surface-normal coordinate nondimensionalized by the *viscous* surface layer scale $\ell_\nu = \nu/u_*$, where $\nu=\mu/\rho$. Equation (4) states that the total stress $T_{\rm tot}(z)$, split between the viscous and inertial contributions on the left-hand side (LHS) and right-hand side (RHS) of Eq. (4), decreases linearly from T_0 at the surface to zero at the channel center plane. Near the surface $(z/\delta \ll 1)$ in the friction-dominated layer $(z^+ \lesssim 5)$, the turbulent stress is negligible $(T_t^+ \ll 1)$ and Eq. (4) is well approximated by

$$\Phi_m(z) \approx \kappa z^+ \quad (z^+ \lesssim 5). \tag{5}$$

This result suggests that $\Phi_m(z)$ exceeds 1 when $z^+ > 1/\kappa \approx 2.5$ (for $\kappa \approx 0.4$), which is well within the friction-dominated portion of the surface layer.

Equation (5) indicates that an overshoot in $\Phi_m(z)$ exists in the smooth-surface high Reynolds number channel flow in a region bounded from below by $z^+ \approx 2.5$ and from above by the lower margin of the inertial LOTW layer and upper margin of the buffer layer. In Fig. 3 we show that this is indeed the case. We replot, in this figure, the data from direct numerical simulations (DNSs) of the smooth wall channel at different Reynolds numbers that has been graciously made available to the scientific community by Iwamoto *et al.*[35,36]

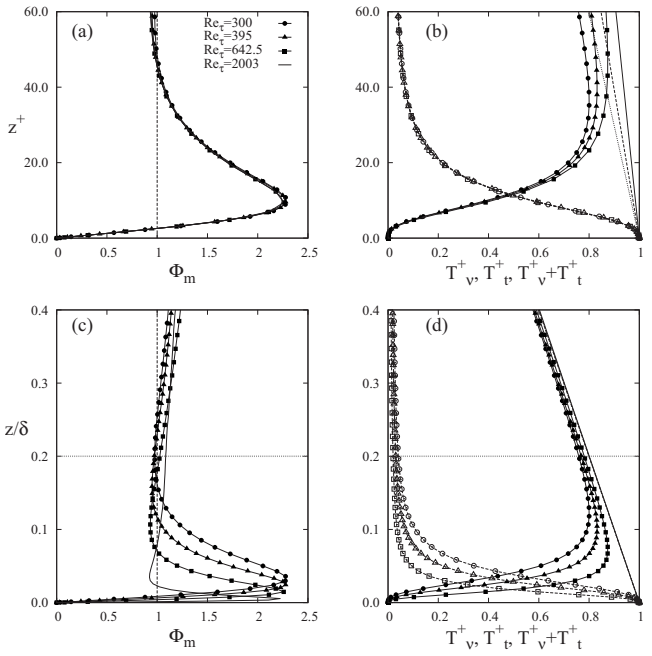

FIG. 3. DNS of the smooth wall channel flow showing the physically real overshoot in the viscous region. (a) Normalized mean shear Φ_m vs z^+. (b) Wall-normalized Reynolds shear stress T_t^+ (filled symbols) and mean viscous shear stress T_ν^+ (open symbols) vs z^+. The dotted, dashed, and thin straight lines are the total shear stress profiles for Reynolds number of 300, 395, and 642, respectively. (c) Φ_m vs z/δ, where δ is the half-channel height. (d) T_t^+ (filled symbols) and T_ν^+ (open symbols) vs z/δ. Total shear stress profiles for three different Reynolds number collapse onto a single linear line. $\kappa=0.4$ is assumed in forming Φ_m. $\mathrm{Re}_\tau=300$, 395, and 642 DNS data are from Iwamoto *et al.* (Ref. 35) and Iwamoto (Ref. 36). In (c) we have added the $\mathrm{Re}_\tau=2003$ DNS data from Hoyas and Jimenez (Ref. 37). The horizontal dotted lines in (c) and (d) indicated the upper margin of the surface layer where LOTW should be predicted.

at $\mathrm{Re}_\tau=300$, 395, and 642, and at $\mathrm{Re}_\tau=2003$ by Hoyas and Jimenez,[37] where $\mathrm{Re}_\tau=u_*\delta/\nu$. Figure 3(a) shows that $\Phi_m(z^+)$ exceeds 1 when z^+ exceeds ≈ 2.5 and peaks at $z^+\approx 10$ with a maximum value of about 2.3 independent of Reynolds number. Φ_m approaches 1 at $z^+\approx 40-50$. Comparing Fig. 3(c) with Fig. 3(d), it is significant that the peak in $\Phi_m(z)$ occurs nearly coincident with the crossover between turbulent stress $T_t(z)$ and viscous stress $T_\nu(z)$. Both the location of overshoot and the location of the crossover occur at $\approx 10\ell_\nu$. Since the position of this overshoot scales on the viscous scale and corresponds to the transition between the dominance of turbulent stress above and viscous stress below, this overshoot reflects the application of an *inertial* length scale z in the portion of the surface layer where the appropriate length scale is the viscous surface scale ℓ_ν. Figures 3(c) and 3(d) show that the overshoot and the crossover in $T_\nu(z)$ and $T_t(z)$ move physically closer to the surface with increasing Reynolds number without a reduction in maximum Φ_m.

B. LES of high Reynolds number turbulent channel flow

We compare the previous analysis with LES of the same high Reynolds number channel flow analyzed in Sec. III A, but in which either a viscous layer exists that is fully unresolved ($\ell_\nu \ll \Delta_z$) or the surface is rough with fully unresolved roughness scale ($z_0 \ll \Delta_z$). The momentum equation for the resolved velocity u_i^r is

$$\frac{\partial u_i^r}{\partial t}+\frac{\partial (u_i^r u_j^r)}{\partial x_j}=-\frac{1}{\rho}\frac{\partial p^r}{\partial x_i}-\frac{\partial \tau_{ij}^{\mathrm{SFS}}}{\partial x_j}, \tag{6}$$

where the viscous force has been scaled out of the momentum balance on account of the high local Reynolds numbers on all grid nodes within the computational domain (surface viscous layers are unresolved or nonexistent). The SFS stress tensor τ_{ij}^{SFS} is modeled. We apply a superscript r to indicate a variable that is carried forward in the simulation as a resolved variable—that is, after the process of explicit and implicit filtering in the algorithmic advancement of the modeled discretized version of Eq. (6). Explicit filtering is generally carried out algorithmically as a dealiasing step [algorithmically, $(u^r u^r)$ in Eq. (6) should be written as $(u^r u^r)^{\hat{r}}$ to indicate the common application of a second explicit filter $\hat{r}$ on the nonlinear term], typically in pseudospectral LES. Implicit filtering arises from the dissipative nature of the model for τ_{ij}^{SFS}, from numerical dissipation within the discretized version of Eq. (6), and from any dissipative elements introduced algorithmically as the discretized dynamical system is advanced in time.

The ensemble mean of Eq. (6) for stationary fully developed high Reynolds number channel flow is

$$\frac{\partial P}{\partial x}=\frac{\partial T_R(z)}{\partial z}+\frac{\partial T_S(z)}{\partial z}=\frac{\partial T_{\mathrm{tot}}(z)}{\partial z} \quad \text{with} \quad \frac{\partial P}{\partial x}=-\frac{\rho u_*^2}{\delta}. \tag{7}$$

The second equation is the global force balance. Total stress $T_{\mathrm{tot}}=T_R+T_S$ is now the summation of a turbulent stress T_R formed from the fluctuating resolved velocity components and the shear component of the mean SFS stress tensor T_S,

$$T_R(z)=-\rho\langle u^{r'} w^{r'}\rangle, \quad T_S(z)=-\rho\langle \tau_{13}^{\mathrm{SFS}}\rangle. \tag{8}$$

Whereas the divergence of the SFS "stress" is physically an inertial contribution to the force balance, in application all SFS models are structured so as to contain a frictional contribution to the equation of motion. This is explicitly true of eddy viscosity models and mixed models which include an eddy viscosity term.

In what follows, we do not restrict our theoretical treatment to any particular SFS stress model. We do, however, use eddy viscosity closures for guidance and to carry out numerical experiments.

We seek a mechanism to extract the frictional component of the complete modeled tensor τ_{ij}^{SFS}; that is, we seek an estimate of a scalar viscosity that extracts the part of τ_{ij}^{SFS} that is parallel to the resolved strain-rate tensor s_{ij}^r in the mean. For the purposes of determining the underlying causes of the overshoot in the highly shear-dominated part of the boundary layer, we define a "LES viscosity" $\nu_{\mathrm{les}}(z)$ as the proportionality between $-\rho\langle \tau_{13}^{\mathrm{SFS}}\rangle$ and $2\langle s_{13}^r\rangle=\partial U/\partial z$,

$$\nu_{\text{les}}(z) \equiv \frac{T_S(z)}{2\rho\langle s_{13}^r\rangle} \quad \text{(closure independent)}, \tag{9}$$

where s_{ij}^r is the resolved strain-rate tensor. Furthermore, since we are focused on the first few grid points adjacent to the surface, we parametrize LES viscosity with its value at the first grid level, $\nu_{\text{LES}}(z_1)$, and we define the normalized LES viscosity as follows:

$$\nu_{\text{LES}} \equiv \nu_{\text{les}}(z_1), \quad \nu_{\text{LES}}^+(z) \equiv \frac{\nu_{\text{les}}(z)}{\nu_{\text{LES}}}. \tag{10}$$

We emphasize that the definitions in Eqs. (9) and (10) do not assume an eddy viscosity model and can be made for *any* closure of the SFS stress tensor. However, this estimate of frictional content is only valid with strong mean shear at the first grid level, and is therefore appropriate to the neutral boundary layer, and the stable and moderately convective ABLs with shear-dominated turbulence at z_1.

Replacing T_S in Eq. (7) with $\rho\nu_{\text{LES}}\nu_{\text{LES}}^+(z)\partial U/\partial z$, integrating in z, and using inertial LOTW scaling [Eq. (1)], produces the expression for $\Phi_m(z)$,

$$\Phi_m(z) = \frac{\kappa z_{\text{LES}}^+}{\nu_{\text{les}}^+(z)}\left(1 - T_R^+(z) - \frac{z}{\delta}\right), \tag{11}$$

where

$$z_{\text{LES}}^+ \equiv \frac{z}{\ell_{\nu_{\text{LES}}}}, \quad \ell_{\nu_{\text{LES}}} \equiv \frac{\nu_{\text{LES}}}{u_*} \quad \text{and} \quad T_R^+ \equiv \frac{T_R}{T_0}. \tag{12}$$

As in the exact channel flow equations, $T_0 = T_{\text{tot}}(0) \equiv \rho u_*^2$, so that $T_R^+(z)$ is the ratio of the resolved part of the Reynolds shear stress to the total wall shear stress. Unlike the viscous layer, where we could argue that the Reynolds stress is a small percentage of wall stress and approximate Eq. (4) by Eq. (2), we cannot *a priori* argue that $T_R \ll T_0$. However, at the first few grid points, $z/\delta \ll 1$ and $\nu_{\text{LES}}^+(z) \sim O(1)$, so that Eq. (11) can be approximated by

$$\Phi_m(z) \approx \kappa z_{\text{LES}}^+(1 - T_R^+) \quad \text{(first few grid points)}. \tag{13}$$

The magnitude of T_R^+ depends on the relative content of resolved to SFS stress in total stress $T_{\text{tot}} = T_R + T_S$. When the separation between resolved and SFSs is in the inertial range, implying that all integral scales are well resolved, then $T_S \ll T_R$, and T_R^+ cannot be neglected in Eq. (13). However, as discussed in Sec. II C, some integral scales are inherently under-resolved at the first few grid levels in high Reynolds number LES of wall-bounded flows. Thus, it may be the case that $T_R^+ \ll 1$ close to the surface so that Eq. (13) is approximated by $\Phi_m(z) \approx \kappa z_{\text{LES}}^+$. If this were the case, then we would reach the same conclusion as when Eq. (4) was reduced to Eq. (5) in the viscous sublayer of the smooth wall channel flow: an overshoot would occur when $z_{\text{LES}}^+ \gtrsim 1/\kappa \approx 2.5$, that is when $z \gtrsim 2.5\ell_{\nu_{\text{LES}}}$.

Figure 4 shows that indeed, $T_S \gg T_R$ near the surface in a typical LES of the neutral ABL (we describe the details of our LESs of the ABL in Appendix B) using the Smagorinsky model, so that $\Phi_m(z) \approx \kappa z_{\text{LES}}^+$ and an overshoot is produced at $z_{\text{LES}}^+ \gtrsim 2.5$. In fact, Figs. 4(a) and 4(b) are very similar to the curves in Figs. 3(a) and 3(b) of the real overshoot in the smooth wall channel flow. The spurious overshoot initiates between the first and second grid levels and peaks nearly coincident with the crossover between T_R and T_S, very similar to Fig. 3, where the real overshoot is found to be coincident with the crossover between T_t and T_ν.

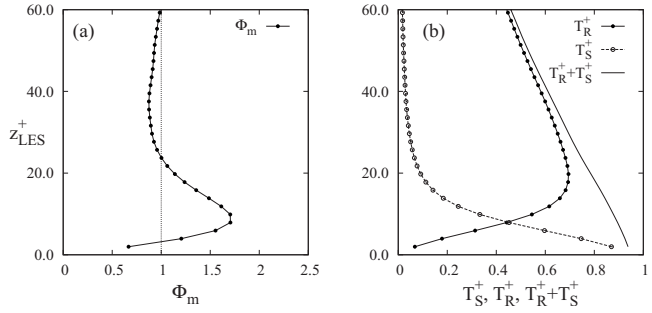

FIG. 4. Overshoot in LES of the neutral ABL using the Smagorinsky model ($C_s = 0.2$) and a $128 \times 128 \times 128$ grid. (a) Φ_m vs z_{LES}^+. (b) Wall normalized mean resolved and SFS shear stress T_R^+ and T_S^+ plotted against z_{LES}^+ and its sum. $\kappa = 0.4$ is assumed in forming Φ_m. $\kappa = 0.4$ is assumed in forming Φ_m.

The overshoot in LES appears to arise from physics similar to the true overshoot in smooth wall channel flow. However, in LES the frictional layer that causes the overshoot is a *numerical* LES frictional layer near the surface that arises from the frictional nature of the modeled SFS stress (and any numerical and algorithmic additions to dissipation). This conclusion is analyzed further in the following sections.

C. The first criterion

The observation from Fig. 4 that the overshoot is associated with a reduction in the resolved Reynolds stress to below the mean SFS stress suggests that the spurious frictional content of the model for SFS stress has introduced a spurious length scale $\ell_{\nu_{\text{LES}}}$ that interferes with the inertial scale z that should dominate the surface layer. The spurious interference of $\ell_{\nu_{\text{LES}}}$ with inertial scaling and the consequent spurious overshoot are essentially the same physics that underlie the production of the real overshoot in the friction-dominated part of the LOTW layer of the smooth wall channel flow. However, unlike the true viscous layer, which is a necessary consequence of frictional force with no slip, the spurious LES frictional layer must be controlled to eliminate the frictionally induced spuriously large mean gradients near the surface. If it were possible to maintain the dominance of T_R over T_S to the surface, then the spurious frictional contribution from the SFS stress model would remain suppressed. This observation suggests a criterion for elimination of the overshoot that

$$\Re \equiv \frac{T_{R_1}}{T_{S_1}} > \Re^* \sim O(1) \quad \text{(closure independent)}, \tag{14}$$

where the subscripts 1 mean "at the first grid level." The critical value $\Re^*$, to be determined experimentally, is an order 1 quantity but may depend on the model for SFS stress, the lower boundary condition, the stability of the ABL, the numerical algorithm, etc.

D. Understanding the ratio $\mathfrak{R}$ and the first criterion

On what does $\mathfrak{R}$ depend and how can it be controlled in a LES? To gain insight into the nature of $\mathfrak{R}$ and find an answer to this question, we develop expressions for $\mathfrak{R}$ based on eddy viscosity representations for the deviatoric part of the SFS stress, $[\tau_{ij}^{\mathrm{SFS}}]_{\mathrm{dev}} \equiv \tau_{ij}^{\mathrm{SFS}} - [\tau_{kk}^{\mathrm{SFS}}/3]\delta_{ij}$,

$$[\tau_{ij}^{\mathrm{SFS}}]_{\mathrm{dev}} = -2\nu_t s_{ij}^r, \quad \nu_t = \ell_t u_t, \tag{15}$$

where ℓ_t and u_t^2 characterize length and energy at the smallest resolved scales. ℓ_t is often taken as a fixed length scale $\ell_t = C_t\Delta$, where $\Delta = (\Delta_x\Delta_y\Delta_z)^{1/3}$ is the grid size ($\Delta_x, \Delta_y, \Delta_z$ are the grid spacings in x, y, z) and C_t is a model constant. Some models embed z-dependence into ℓ_t in the form $\ell_t(z) = C_t\tilde{\ell}_t(z)$, where $\tilde{\ell}_t(z)$ is specified to decrease toward the surface and approaches Δ away from the surface.[1] Dynamic models take $\ell_t = C_t\Delta$, but determine C_t dynamically with the result that $C_t = C_t(z)$ reduces near the surface.[4] Thus, in each case the modeled length scale $\ell_t(z)$ decreases toward the surface. In the current work we develop scaling from eddy viscosity closures with constant $\ell_t = C_t\Delta$, but shall discuss our results in context with z-dependent ℓ_t in the Discussion, Sec. VII B.

The space-time variability in $\nu_t(\mathbf{x},t)$ is modeled through a fluctuating velocity scale $u_t(\mathbf{x},t)$, given for the Smagorinsky closure by $u_{t,\mathrm{Smag}}(\mathbf{x},t) = \Delta(2s_{ij}^r s_{ij}^r)^{1/2}$. In the basic one-equation model, $u_{t,\text{1-eq}}(\mathbf{x},t) = \sqrt{e(\mathbf{x},t)}$, where $e(\mathbf{x},t)$ represents the SFS kinetic energy, modeled through a prognostic equation.[32,38] In both models $\ell_t = C_t\Delta$. Here we develop expressions using the Smagorinsky closure with C_t replaced by C_s^2, as is traditional. However we shall present results for both the Smagorinsky and one-equation eddy viscosity models.

Independent of the model, $[\tau_{13}^{\mathrm{SFS}}]_{\mathrm{dev}} = \tau_{13}^{\mathrm{SFS}}$ and

$$T_{S_1} = -\rho\langle\tau_{13}^{\mathrm{SFS}}\rangle_1 \equiv 2\rho\nu_{\mathrm{LES}}\langle s_{13}^r\rangle_1 = 2\rho\xi_1\langle\nu_t\rangle_1\langle s_{13}^r\rangle_1, \tag{16}$$

where

$$\nu_{\mathrm{LES}} = \xi_1\langle\nu_t\rangle_1 \quad \text{with} \quad \xi_1 = \left(1 + \frac{\langle\nu_t' s_{13}^{r\prime}\rangle_1}{\langle\nu_t\rangle_1\langle s_{13}^r\rangle_1}\right). \tag{17}$$

We have found from LES of the neutral ABL that ξ_1 is typically ≈ 1.05. The ensemble mean of the eddy viscosity at the first grid level with the Smagorinsky closure is

$$\langle\nu_t\rangle_1 = C_s^2\Delta^2\langle(2s_{ij}^r s_{ij}^r)^{1/2}\rangle_1 \approx 2C_s^2\Delta^2\langle s_{13}^r\rangle_1 = C_s^2\Delta^2\left(\frac{\partial U}{\partial z}\right)_1, \tag{18}$$

where

$$\langle(s_{ij}^r s_{ij}^r)^{1/2}\rangle_1 \approx \sqrt{2}\langle s_{13}^r\rangle_1\left(1 + \frac{1}{8}\frac{\langle s_{ij}^{r\prime} s_{ij}^{r\prime}\rangle_1}{\langle s_{13}^r\rangle_1^2}\right)$$

is well approximated by $\sqrt{2}\langle s_{13}^r\rangle_1$ since the strain-rate fluctuations are nearly all SFS (this is especially true at the first grid level where the integral scales are minimally or poorly resolved). We write the mean streamwise velocity gradient in a form appropriate for inertial scaling in the surface layer:

$$2\langle s_{13}^r\rangle_1 = \left(\frac{\partial U}{\partial z}\right)_1 \equiv \frac{u_*}{\tilde{\kappa}_1 z_1}. \tag{19}$$

In Eq. (19) $\tilde{\kappa}_1$ is defined as the value required to make the LHS equal to the RHS at the first grid level. Only if LOTW is predicted by the LES, so that $\tilde{\kappa}_1$ is constant through the surface layer, will $\tilde{\kappa}_1$ be the predicted value of the von Kármán constant. [When the Coriolis force is present, as in LES of the ABL, the velocity at the first grid level is at an angle θ_1 to the geostrophic wind velocity above the boundary layer. In this case, Eqs. (19)–(21), (23), (24), (27), and (28) contain an additional factor $\cos\theta_1$, as given in Appendix A.]

Inserting Eq. (19) into Eqs. (18) and (17) leads to the following expression for the LES viscosity:

$$\nu_{\mathrm{LES}} = \frac{\xi_1}{\tilde{\kappa}_1} D_s u_* \Delta_z, \quad \text{where}$$
$$D_s \equiv C_s^2 A_R^{4/3} \quad (\text{Smagorinsky}). \tag{20}$$

$A_R = \Delta_x/\Delta_z = \Delta_y/\Delta_z$ is the aspect ratio of the grid and $\Delta_z = z_1$ is the vertical grid spacing. As will be discussed at length, Eq. (20) indicates that the LES viscosity is proportional to the combination $C_s^2 A_R^{4/3}$, and therefore is altered both by the constant in the SFS model and by the aspect ratio of the grid, as well as by the vertical grid spacing.

Applying Kolmogorov scaling[39] and LOTW scaling to the one-equation model produces a result similar to Eq. (20), but with D_s replaced by $D_k = C_k A_R^{8/9}$, where C_k is the model constant, and with $\tilde{\kappa}_1$ replaced by a different order one constant β. The main point is that with the eddy viscosity closure, the LES viscosity is proportional to the product of model constant and grid aspect ratio, each raised to a power that depends on the closure.

In order to develop an expression for $\mathfrak{R}$, we note that since the total shear stress is $T_{\mathrm{tot}} = T_R + T_S$, $\mathfrak{R}$ is given by

$$\mathfrak{R} = \frac{T_{\mathrm{tot}_1}}{T_{S_1}} - 1 = \frac{\xi_2(\rho u_*^2)}{T_{S_1}} - 1 \quad (\text{closure independent}), \tag{21}$$

where

$$\xi_2 \equiv \frac{T_{\mathrm{tot}_1}}{T_{\mathrm{tot}_0}} \approx \frac{N_\delta - 1}{N_\delta}. \tag{22}$$

In Eqs. (21) and (22) $T_{\mathrm{tot}_0} = \rho u_*^2$ and $N_\delta = \delta/\Delta_z$ is the number of grid points from the surface to the top of the boundary layer. ξ_2 is generally very close to 1.

Inserting Eq. (19) for $\langle s_{13}^r\rangle_1$ and Eq. (20) for ν_{LES} into $T_{S_1} = 2\rho\nu_{\mathrm{LES}}\langle s_{13}^r\rangle_1$, and then inserting this result for T_{S_1} into Eq. (21), produces

$$\mathfrak{R} = \frac{\xi\beta\tilde{\kappa}_1}{D_t} - 1 \quad (\text{eddy viscosity}), \tag{23}$$

where $\xi \equiv \xi_2/\xi_1$ is generally very close to 1. For the Smagorinsky closure, $\beta = \tilde{\kappa}_1$ and $D_t \to D_s = C_s^2 A_R^{4/3}$, whereas for the one-equation model $D_t \to D_k = C_k A_R^{8/9}$ and β is a different order one constant.

The eddy viscosity closure was used in the derivation of Eq. (23) to provide insight into the mechanisms underlying $\Re$ and how it can be systematically adjusted in LES in order to move the LES into the supercritical regime $\Re > \Re^*$. We learn that the ratio of resolved to SFS stress at the first grid level can be increased either by reducing the model constant or by reducing the grid aspect ratio in the combination

$$D_t = C_t^a A_R{}^b, \tag{24}$$

The model constant C_t [Eq. (15)] and A_R enter in this combination through the LES viscosity, Eq. (20), and the powers a and b are model dependent. Thus, LES viscosity can be decreased and $\Re$ increased by reducing either or both C_t and A_R to reduce D_t.

The explanation behind the effects of model constant and A_R on $\Re$ is in the manner that each reduction affects the balance between resolved and SFS stress within the total stress $T_{\text{tot}}(z)$ that is fixed by the global momentum balance. Reducing the model constant directly reduces the average SFS stress T_S. Reducing the aspect ratio corresponds to an increase in resolution in the horizontal, which moves vertical velocity variance and Reynolds stress from SFSs to resolved scales in the horizontal. The consequence of both effects is to reduce T_S relative to T_R, and therefore to increase the ratio $\Re = T_{R_1}/T_{S_1}$. Similarly, both effects reduce LES viscosity.

IV. THE BALANCE BETWEEN NUMERICAL FRICTION AND INERTIA: A SECOND OBSERVATION

The above discussion suggests that the mechanisms that underlie the generation of a mean gradient overshoot and its consequences are associated with numerical LES friction that, in the modeled dynamical system, forces a physical response similar to that underlying the overshoot in Newtonian turbulent channel flow (Fig. 3) that results from *molecular friction*. Like the real viscous layer in smooth wall channel flow that arises from a change in scaling from z to $\ell_\nu = \nu/u_*$, the overshoot in LES reflects a transition in dominance from the inertial surface scale z to a numerical LES viscous length scale $\ell_{\nu_{\text{LES}}} = \nu_{\text{LES}}/u_*$ that dominates near the surface. LES produces an overshoot in $\Phi_m(z)$ as a result of the spurious dominance of the length scale $\ell_{\nu_{\text{LES}}}$ in a region where the integral scales should scale on z.

However, for the LOTW to exist in an inertia-dominated surface layer, inertial effects must be sufficiently strong relative to viscous forces, as measured by the ratio of the boundary layer depth to the viscous wall scale, the Reynolds number $\text{Re}_\tau = \delta/\ell_\nu$. This suggests the existence of a "LES Reynolds number" $\text{Re}_{\text{LES}} = \delta/\ell_{\nu_{\text{LES}}}$. Since friction in the discretized LES dynamical system is at the core of the overshoot, we must consider all consequences of friction, including the requirement that inertial effects dominate viscous effects sufficiently to produce the LOTW scaling, $\partial U/\partial z \sim u_*/z$.

In particular, in the smooth wall channel flow the inertial layer will only reflect the LOTW when inertia dominates the viscous force within the surface layer sufficiently that Re_τ exceeds a critical value Re_τ^*. The DNS data of Fig. 3 show

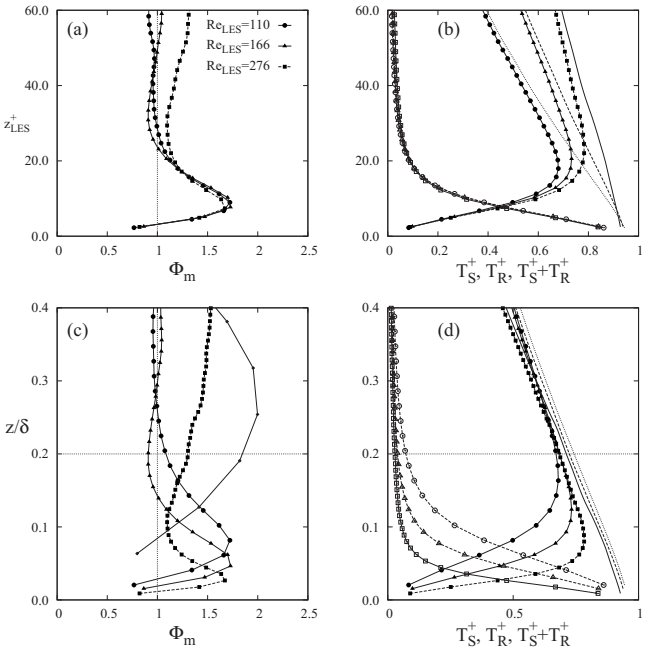

FIG. 5. Overshoots in LES of the neutral ABL. (a) Φ_m vs z^+_{LES}. (b) Normalized resolved Reynolds stress T_R^+ (filled symbols) and mean SFS shear stress T_S^+ (open symbols) vs z^+_{LES}. Dotted, dashed, and thin lines are the sum of resolved and SFS stress from low to high LES Reynolds number. (c) Φ_m vs z/δ, where δ is defined as the height where $\Phi_m = 0$. (d) T_R^+ (filled symbols) and T_S^+ (open symbols) vs z/δ. The LES Reynolds numbers of the simulations are shown in (a). In order of Re_{LES}, the Smagorinsky constants and grids were ($C_s = 0.1$, $42 \times 42 \times 96$), ($C_s = 0.2$, $192 \times 192 \times 128$), and ($C_s = 0.1$, $128 \times 128 \times 256$). The thin black line in (c) is a simulation with such low Re_{LES} that turbulence is barely sustained ($C_s = 0.2$, $42 \times 42 \times 32$ and $\text{Re}_{\text{LES}} = 38$). The horizontal dotted lines in (c) and (d) indicated the upper margin of the surface layer where LOTW should be predicted. $\kappa = 0.4$ is assumed in forming Φ_m.

that the LOTW is not captured in the viscous channel flow even at $\text{Re}_\tau = 2003$, when the viscous layer (defined by the peak in Φ_m) is only 2% of the surface layer.

Similarly, one can expect that LES of the high Reynolds number boundary layer can only produce LOTW scaling when inertia in the discretized dynamical system dominates friction sufficiently that the LES Reynolds number Re_{LES} exceeds some critical value, Re^*_{LES}. Indeed one can also postulate a transitional Re_{LES} which must be exceeded to support turbulence in the discretized LES dynamical system. In Fig. 5 we show four LESs of the ABL at increasing values of Re_{LES}. Similar to Fig. 3 for DNS of channel flow where the peak in the overshoot scales on the viscous scale ℓ_ν, with the exception of the lowest Re_{LES} (thin solid curve with small dots), the overshoot in LES scales on the numerical LES viscous scale, $\ell_{\nu_{\text{LES}}}$ [Fig. 5(a)]. In fact, both the true channel flow overshoot and the spurious LES overshoot peak at ten corresponding viscous units. Thus, the LES overshoot moves closer to the surface along with $\ell_{\nu_{\text{LES}}}$ as $\text{Re}_{\text{LES}} = \delta/\ell_{\nu_{\text{LES}}}$ increases [Fig. 5(c)] and the numerical LES viscous layer occupies a correspondingly smaller percentage of the surface layer. Similarly, the peak in $\Phi_m(z)$ coincides with the crossover between mean resolved and SFS stress T_R and T_S [Fig. 5(d)] so that the crossover also scales on $\ell_{\nu_{\text{LES}}}$ [Fig. 5(b)].

The thin solid curve (with small dots) in Fig. 5(c) is

included to illustrate the consequence of a LES Reynolds number that is too low to support turbulence. The mean velocity profile is qualitatively similar to the parabolic profile characteristic of laminar Newtonian channel flow. Thus, although the LES equation contains no true frictional term, the numerical LES friction inherent in the model and adjusted by the grid as described by ν_{LES} in Eq. (20) can, like real friction, dampen inertial motions and prevent turbulence within the discretized dynamical system advanced in the LES.

The frictional content of the simulation embodied by ν_{LES} should, in principle, be extended to include the numerical dissipation within the specific discretization that is applied to advance the LES equations in time with a SFS model. The LES presented in Sec. VI applies the pseudospectral method in the horizontal and finite difference in the vertical on a staggered mesh and is minimally dissipative. Significant frictional content within the numerical algorithm might strengthen the overshoot beyond what is described here.

A. The second and third criteria

The first criterion discussed in Sec. III C is a necessary condition to eliminate the overshoot but is not a sufficient condition to correctly predict LOTW scaling in the high Reynolds number surface layer—that is, constant $\phi(z)$ is the surface layer. A second criterion is necessary: that $\mathrm{Re}_{\mathrm{LES}}$ exceed a critical $\mathrm{Re}^*_{\mathrm{LES}}$ to achieve LOTW scaling in the simulated dynamical system. In the presence of the overshoot, one would expect that to predict the LOTW in the part of the surface layer that is not directly affected by numerical LES friction, $\mathrm{Re}^*_{\mathrm{LES}}$ would have to achieve values in thousands similar to Re^*_τ in real frictional channel flow. However, unlike the DNS of channel flow, where the overshoot is real and cannot be eliminated, in LES of high Reynolds number boundary layers the overshoot and its frictional sources are spurious. Therefore, the critical Reynolds number $\mathrm{Re}^*_{\mathrm{LES}}$ required to satisfy the second criterion turns out to be much lower when $\mathfrak{R}>\mathfrak{R}^*$ (and the overshoot is eliminated) than when the overshoot is maintained as in Fig. 5.

To show this we use Eq. (19) to write

$$T_{S_1} = 2\rho\nu_{\mathrm{LES}}\langle s^r_{13}\rangle_1 = \rho\nu_{\mathrm{LES}}\frac{u_*}{\tilde{\kappa}_1 z_1} \quad \text{(closure independent)}. \tag{25}$$

Inserting Eq. (25) into Eq. (21) yields an expression for $\mathrm{Re}_{\mathrm{LES}}$ that is valid independent of the SFS model

$$\mathrm{Re}_{\mathrm{LES}} = \frac{N_\delta}{\xi_2\tilde{\kappa}_1}(\mathfrak{R}+1) \quad \text{(closure independent)}. \tag{26}$$

Thus $\mathrm{Re}_{\mathrm{LES}}$ depends both on $\mathfrak{R}$ and on the vertical grid resolution N_δ. [Note that in Fig. 5(c) the LES given by the solid curve has low $\mathrm{Re}_{\mathrm{LES}}$ because of low vertical grid resolution.] The critical LES Reynolds number $\mathrm{Re}^*_{\mathrm{LES}}$ is therefore associated not only with the critical ratio of resolved to SFS stress $\mathfrak{R}^*$, but also with a critical vertical resolution N^*_δ, where

$$\mathrm{Re}^*_{\mathrm{LES}} = \frac{N^*_\delta}{\xi_2\tilde{\kappa}_1}(\mathfrak{R}^*+1) \quad \text{(closure independent)}. \tag{27}$$

The third criterion, that N_δ exceed a critical value N^*_δ, follows from the second criterion, $\mathrm{Re}_{\mathrm{LES}}>\mathrm{Re}^*_{\mathrm{LES}}$ when $\mathfrak{R}\geq\mathfrak{R}^*$.

One way to understand the requirement for a minimum vertical resolution to produce high accuracy LES of the boundary layer is simply as a manifestation of the standard computational requirement that all special regions with their own characteristic dynamics be well resolved for accurate numerical simulation. The surface layer is an example of a region with special dynamics that requires good resolution. The surface layer occupies 15%–20% of the boundary layer depth at high Reynolds numbers. Resolving this layer with, say, ten grid points in the vertical therefore leads to an estimate for N^*_δ of $\sim$50–65. Recognizing that $\mathfrak{R}^*$ and $\mathrm{Re}^*_{\mathrm{LES}}$ are model dependent, we can estimate $\mathrm{Re}^*_{\mathrm{LES}}$ roughly for $\mathfrak{R}^*\approx 1$ to be $\mathrm{Re}^*_{\mathrm{LES}}\sim 250$–325. This estimate assumes that the overshoot has been eliminated and that the LOTW has been captured with $\tilde{\kappa}_1=\kappa\approx 0.4$. That is, we assume that there are no additional confounding influences that cause the LES to deviate from the LOTW. (In Sec. VII we shall discuss confounding influences.) This estimate for $\mathrm{Re}^*_{\mathrm{LES}}$ is well over an order of magnitude *lower* than what we would estimate by analogy with Re^*_τ in DNS of channel flow if the overshoot were retained, but confined to a sufficiently thin, numerically viscous layer adjacent to the surface.

We shall find (Sec. VI) that for our current LES of the ABL with the Smagorinsky eddy viscosity closure, 45–50 is a reasonable estimate for N^*_δ and 350 is a reasonable estimate for $\mathrm{Re}^*_{\mathrm{LES}}$. The good news is that a vertical grid resolution $N_z\approx 2N^*_\delta\sim 90$–100 is not overly severe and doable on current mainframes. The bad news is that most calculations in the literature are of LES with vertical resolutions below critical. Interestingly, we shall show in Sec. V B that in addition to subcritical resolution in the vertical, there are practical limitations to the maximum vertical resolution in LES of the high Reynolds number boundary layer.

B. Understanding the LES Reynolds number and the three criteria

To develop greater insight into the LES Reynolds number and its control, we evaluate $\mathrm{Re}_{\mathrm{LES}}=\delta/\ell_{\nu_{\mathrm{LES}}}$ using the Smagorinsky eddy viscosity representation for the SFS stress, as was done to understand $\mathfrak{R}$ in Sec. III D. There we derived an expression for the LES viscosity ν_{LES} [Eq. (20)]. Using this expression, the numerical LES viscous length scale is given by

$$\ell_{\nu_{\mathrm{LES}}} \equiv \frac{\nu_{\mathrm{LES}}}{u_*} = \frac{\xi_1}{\beta}D_t\Delta_z \quad \text{(eddy viscosity)}, \tag{28}$$

where $\beta=\tilde{\kappa}_1$ for the Smagorinsky closure. Dividing δ by Eq. (28), or replacing $\mathfrak{R}$ in Eq. (26) by Eq. (23), produces the following expression for the LES Reynolds number:

$$\mathrm{Re}_{\mathrm{LES}} = \frac{\beta}{\xi_1}\frac{N_\delta}{D_t} \quad \text{(eddy viscosity)}. \tag{29}$$

Several interesting observations can be extracted from Eqs. (28) and (29). Since the overshoot scales on $\ell_{\nu_{\mathrm{LES}}}$ and peaks at $10\ell_{\nu_{\mathrm{LES}}}$ (Fig. 5), the observation made in Sec. II C from previous studies—that the overshoot is tied to the grid—can now be explained. Equation (28) shows that if neither the model constant nor the grid aspect ratio is altered while the grid is refined, the LES viscous scale $\ell_{\nu_{\mathrm{LES}}}$, and therefore the peak in Φ_m, will move closer to the surface in proportion to the grid spacing Δ_z. However, since $D_t = C_t^a A_R^b$ is left unchanged during the grid refinement, $\mathfrak{R}$ and the magnitude of the overshoot will not change—the overshoot simply moves closer to the surface, as shown in Figs. 3 and 5. In particular, Fig. 5 shows that as the overshoot moves toward the surface in proportion to the grid spacing at constant A_R and C_t, the ratio $T_{R_1}/T_{S_1} = \mathfrak{R}$ and magnitude of peak Φ_m remain unchanged, and the locations of peak Φ_m remain attached to the crossover between T_R and T_S.

A second interpretation follows by replacing $\mathrm{Re}^*_{\mathrm{LES}}$ with $\delta/\ell^*_{\nu_{\mathrm{LES}}}$ in Eq. (27). The criterion $\mathfrak{R} > \mathfrak{R}^* \approx 1$ is then equivalent to

$$\frac{\ell_{\nu_{\mathrm{LES}}}}{\Delta_z} < \frac{\ell^*_{\nu_{\mathrm{LES}}}}{\Delta_z} = \frac{\xi_2 \tilde{\kappa}_1}{\mathfrak{R}^* + 1} \sim 0.2 \quad \text{(closure independent)}. \tag{30}$$

Equation (30) states that the spurious length scale $\ell_{\nu_{\mathrm{LES}}}$ arising from friction within the SFS model and grid underresolution in a LES must be confined sufficiently well within the first grid cell for numerical LES friction to not adversely affect the LES. Note that Eq. (30) is equivalent to the requirement that $z^+_{1_{\mathrm{LES}}} \gtrsim 5$: the first grid level must be at least five times larger than the spurious viscous length scale.

The inequality (30) is satisfied when $\mathfrak{R} > \mathfrak{R}^*$, so that the first and second criteria are met when the spurious viscous length scale is sufficiently small relative to the grid spacing. However Eq. (30) does not guarantee the third criterion $N_\delta > N^*_\delta$. This is because the overshoot peaks at $10\ell_{\nu_{\mathrm{LES}}}$, so that the condition given by Eq. (30) still allows partial resolution of the overshoot (e.g., when $10\ell_{\nu_{\mathrm{LES}}}/\Delta_z \sim 2$). One can therefore interpret the addition of the third criterion $N_\delta > N^*_\delta$ as demanding that the spurious frictional length scale $\ell_{\nu_{\mathrm{LES}}}$ be buried both sufficiently far within the first grid level Δ_z and within the boundary layer δ that the grid is given no opportunity to either create an overshoot or alter LOTW scaling through the influence of friction within the surface layer.

V. A FRAMEWORK FOR HIGH-ACCURACY LARGE-EDDY SIMULATION: THE "HIGH-ACCURACY ZONE"

By comparing Eq. (23) for $\mathfrak{R}$ with Eq. (29) for $\mathrm{Re}_{\mathrm{LES}}$ we learn that reducing the model constant and/or the grid aspect ratio in the combination $D_t = C_t^a A_R^b$ causes both $\mathfrak{R}$ and $\mathrm{Re}_{\mathrm{LES}}$ to increase (and, correspondingly, $\ell_{\nu_{\mathrm{LES}}}/\Delta_z$ to decrease). However, increasing only the vertical resolution increases the LES Reynolds number but has no effect on the ratio of resolved to SFS stress $\mathfrak{R}$. This observation leads to the concept of a "$\mathfrak{R} - \mathrm{Re}_{\mathrm{LES}}$ parameter space" in which high-accuracy LES of the high Reynolds number boundary layer could be developed. Within this framework, one can systematically adjust the LES of the boundary layer so that, in the high Reynolds number limit, the overshoot is suppressed and the LOTW is captured. The $\mathfrak{R} - \mathrm{Re}_{\mathrm{LES}}$ parameter space is illustrated in Fig. 6; a LES of the boundary layer is identified as a point on a plot of $\mathfrak{R}$ against $\mathrm{Re}_{\mathrm{LES}}$. In subsequent simulations, the LES is adjusted to move the point within the $\mathfrak{R} - \mathrm{Re}_{\mathrm{LES}}$ parameter space relative to the critical parameters $\mathfrak{R}^*$, $\mathrm{Re}^*_{\mathrm{LES}}$, and N^*_δ.

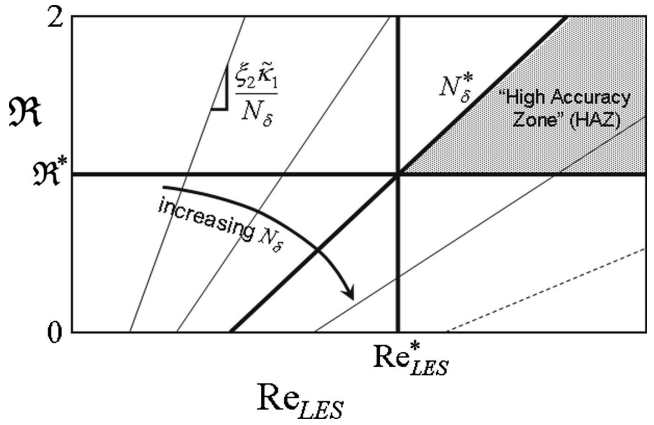

FIG. 6. Schematic of the structure of the $\mathfrak{R} - \mathrm{Re}_{\mathrm{LES}}$ parameter space. This parameter space underlies the framework we propose for designing a LES that is capable of predicting LOTW scaling for $\partial U/\partial z$.

For the LES to capture the LOTW while resolving the overshoot, the simulation must live in the rectangular space $\mathfrak{R} > \mathfrak{R}^*$, $\mathrm{Re}_{\mathrm{LES}} > \mathrm{Re}^*_{\mathrm{LES}}$. We have roughly estimated $\mathfrak{R}^* \sim 1$ and $\mathrm{Re}^*_{\mathrm{LES}} \sim 350$. However in addition to the criteria $\mathfrak{R} > \mathfrak{R}^*$ and $\mathrm{Re}_{\mathrm{LES}} > \mathrm{Re}^*_{\mathrm{LES}}$, we have argued for a third criterion $N_\delta > N^*_\delta$. $\mathfrak{R}$ and $\mathrm{Re}_{\mathrm{LES}}$ are linearly related by Eq. (26),

$$\mathfrak{R} = \left(\frac{\xi_2 \tilde{\kappa}_1}{N_\delta}\right) \mathrm{Re}_{\mathrm{LES}} - 1 \quad \text{(closure independent)}. \tag{31}$$

Thus, N_δ enters in the slope of $\mathfrak{R}$ versus $\mathrm{Re}_{\mathrm{LES}}$. In Fig. 6 we plot Eq. (31) as a series of lines with constant slope $\xi_2\tilde{\kappa}_1/N_\delta$. Since LOTW is only captured in the supercritical region of the $\mathfrak{R} - \mathrm{Re}_{\mathrm{LES}}$ parameter space, in general $\tilde{\kappa}_1$ will vary from point to point on lines of constant slope $\xi_2\tilde{\kappa}_1/N_\delta$. However the variation in $\tilde{\kappa}_1$ is not so great as to obscure the strong inverse relationship between the slopes of the $\mathfrak{R} - \mathrm{Re}_{\mathrm{LES}}$ lines and the vertical grid resolution N_δ. It can be shown from Eq. (27) that the third criterion $N_\delta > N^*_\delta$ is met when the simulation lies to the right of the $\mathfrak{R} - \mathrm{Re}_{\mathrm{LES}}$ line with slope $\xi_2\tilde{\kappa}_1/N^*_\delta$ that passes through the intersection between $\mathfrak{R} = \mathfrak{R}^*$ and $\mathrm{Re}_{\mathrm{LES}} = \mathrm{Re}^*_{\mathrm{LES}}$, as illustrated in Fig. 6. We call the wedge-shaped region that defines supercritical LES satisfying all three criteria $\mathfrak{R} > \mathfrak{R}^*$, $\mathrm{Re}_{\mathrm{LES}} > \mathrm{Re}^*_{\mathrm{LES}}$, and $N_\delta > N^*_\delta$ the "high accuracy zone" (HAZ). The LES must reside within the HAZ to meet the three criteria required to both eliminate the overshoot and capture the LOTW.

A. Designing LES to capture law-of-the-wall scaling

The objective is to systematically move the LES into the HAZ of the $\Re-\mathrm{Re}_{\mathrm{LES}}$ parameter space by combining Eq. (31) with knowledge gained from Eqs. (23) and (29). Although we have applied eddy viscosity closures to gain insight into the process of adjusting N_δ, $\Re$, and $\mathrm{Re}_{\mathrm{LES}}$ to systematically move the LES within the $\Re-\mathrm{Re}_{\mathrm{LES}}$ parameter space, the basic method can be applied with any SFS stress model. T_{R_1} and T_{S_1} (and therefore $\Re$) and ν_{LES} (and therefore $\mathrm{Re}_{\mathrm{LES}}$) can be quantified independently of the SFS model, the only requirement being that all contributions to the SFS stress are included in defining τ_{ij}^{SFS} before calculating T_{S_1}. This relatively simple process may be described in two basic steps.

(1) Adjust, and hold fixed, the vertical resolution of the grid (N_z) so that when the simulation is fully developed, N_δ will exceed N_δ^* (typically, $N_z \sim 1.5N_\delta - 2N_\delta$ to minimize the influence of the upper boundary condition). We shall point out that it is possible to over-resolve in the vertical.
(2) Then systematically adjust the aspect ratio of the grid together with the model constant to move the simulation roughly along a straight line in Fig. 6 from the subcritical region of the $\Re-\mathrm{Re}_{\mathrm{LES}}$ parameter space into the HAZ. With eddy viscosity closures, the model constant and aspect ratio appear in the combination $D_t=C_t^a A_R{}^b$. However, to move into the HAZ with any other closure, one would adjust the model constant for that closure (to systematically reduce the SFS stress) together with a systematic increase in the horizontal resolution of the grid (to systematically reduce the aspect ratio).

We presume that the closure for SFS stress relies on a dissipative mechanism to model the net transfer of resolved turbulence energy to SFS motions. With this methodology for designing LES one can analyze systematically what works better or worse depending on the choice of model type, model details, model constant, grid resolution, grid structure, algorithm, geometry, etc., with some understanding of underlying mechanisms. This framework provides the LES community with both physical understanding and structure upon which a systematic procedure for LES design may be based. Once the researcher has become experienced with the method, she/he will be able to design high-accuracy LES more rapidly using her/his favorite SFS model, algorithm, code, etc.

Whereas the model constant C_t and the model length scale $\ell_t=C_t\Delta$ are uniform in the above discussions, in the general eddy viscosity model the length scale ℓ_t is specified as varying with z. The Mason and Thomson[1] modification of the length scale ℓ_t near the surface and the dynamic procedure that adjusts the Smagorinsky constant C_s with z (e.g., Porté-Agel *et al.*[4]) are examples. The primary issue is that the level of eddy viscosity be adjusted in concert with the grid aspect ratio (i.e., the horizontal resolution of vertical motions) within the first few grid levels from the surface, where under-resolution is of primary concern and mean SFS stress competes with resolved stress.

B. Grid-independent LES and practical limits on grid resolution

As discussed in Sec. II C, a problem with current LES of the ABL is grid dependence in the mean flow. We shall show in Sec. VI that as the simulation moves systematically into the HAZ within the $\Re-\mathrm{Re}_{\mathrm{LES}}$ parameter space, a grid-independent solution for the mean velocity is achieved. However, one cannot move the simulation infinitely far into the HAZ along lines of fixed vertical grid resolution N_δ, since that would require that either the model constant be driven to zero (removing the model from the dynamical system) or the grid aspect ratio would be taken to zero (creating infinitesimally thin grid cells and large computational expense). Either of these limits will cause numerical problems and simulation error regardless of computational expense. Thus, for both accuracy and practical reasons, the optimal location for the simulation within the HAZ is near the apex of the wedge in Fig. 6 where $\Re \gtrsim \Re^*$, $\mathrm{Re}_{\mathrm{LES}} \gtrsim \mathrm{Re}_{\mathrm{LES}}^*$, and $N_\delta \gtrsim N_\delta^*$.

Similarly there are practical limits on vertical resolution that surprisingly confine the growth of LES grids on any given computer. Although a minimum vertical resolution is required to move the simulation into the HAZ, progressive increases in vertical resolution will force the simulation onto lines in the $\Re-\mathrm{Re}_{\mathrm{LES}}$ parameter space that have progressively smaller slopes, as illustrated by the dashed line in Fig. 6. Increases in vertical grid resolution in the absence of other adjustments will increase the grid aspect ratio, driving $\Re$ to subcritical values and restoring the overshoot along with its related errors. With eddy viscosity models, for example, in order that $\Re \approx \Re^*$ as N_δ is increased, $D_t=C_t^a A_R^b$ must be held constant [Eq. (23)]. However, since the minimum model constant and maximum grid aspect ratio are bounded, grid aspect ratio must, at some point, be maintained roughly fixed with increasing vertical resolution, and horizontal grid resolution must increase proportionally with N_δ. The number of grid points will therefore increase approximately as N_δ^3, severely limiting the vertical resolution to modest values. This dilemma is reminiscent of DNS where the highest Reynolds number that can be simulated accurately grows slowly with increasing computer size due to the rapid increase in resolution requirements with increasing Reynolds number.

VI. NUMERICAL EXPERIMENTS

To evaluate the theory and further explore the application of the $\Re-\mathrm{Re}_{\mathrm{LES}}$ framework to the development of wall bounded LES, we have carried out over 110 LESs of the neutral shear-driven ABL capped with an inversion layer to suppress boundary layer growth and produce a quasistationary long-time solution. The Coriolis force is included at a relatively high level to reduce the time to reach quasistationary, so the mean wind is skewed relative to the geostrophic wind (x direction) at the first grid level (see Appendix A). The code is pseudospectral in the horizontal and finite difference in the vertical, so numerical dissipation is minimal. In the horizontal statistically homogeneous directions we apply periodic boundary conditions; in the vertical we apply the boundary conditions, as described by Moeng[38] and Sullivan

et al.[40] We report here on simulations with the Smagorinsky closure and uniform grid spacing. In particular, we apply the nonlinear Moeng[38] model for total fluctuating shear stress at the lower surface and the friction velocity is made proportional to the mean wind at the first grid level with a proportionality constant that can be related to the surface roughness length scale z_0. A summary of the numerical algorithm and simulations is given in Appendix B and in several publications.[2,21,38,40]

It should be noted that in our code, dealiasing in the horizontal directions is carried out by padding rather than truncation. These are equivalent except in the interpretation of the grid and grid length scale: the grid resolutions and aspect ratios quoted in the figures are *before* padding and the grid length scale $\Delta=(\Delta_x\Delta_y\Delta_z)^{1/3}$ used in the eddy viscosity model [Eq. (15)] is also based on the prepadded grid. In all plots we define the boundary layer thickness δ at the height where the mean velocity gradient crosses zero. Whereas the number of grid points in the vertical N_z is defined before the simulation, the number of grid points within the boundary layer N_δ is determined after a simulation is analyzed in the quasistationary state. We were careful to determine the quasistationary state consistently in all simulations (see Appendix B). In all plots of $\Phi_m(z)=\kappa\phi(z)$ we use a value of 0.40 for κ.

A. The $\Re-\mathrm{Re}_{\mathrm{LES}}$ parameter space

In Fig. 7 we identify in the $\Re-\mathrm{Re}_{\mathrm{LES}}$ parameter space all the simulations carried out for the current study. As will be discussed below, from the predictions of $\Phi_m(z)$ we estimated the critical lines $\Re=\Re^*$, $\mathrm{Re}_{\mathrm{LES}}=\mathrm{Re}^*_{\mathrm{LES}}$, and $N_\delta=N^*_\delta$ drawn on the figures. In Fig. 7(a) different symbols are used according to the number of grid points in the vertical N_z ($\approx 1.5N_\delta$). These show approximate correspondence to the straight line representations of Eq. (31) in Fig. 6 at constant slope $(\xi_2\tilde{\kappa}_1/N_\delta)$. Note that the points in Fig. 7(a) become noticeably more linear as the simulations enter the triangular HAZ region of the $\Re-\mathrm{Re}_{\mathrm{LES}}$ parameter space and $\tilde{\kappa}_1$ better represents the von Kármán constant. To demonstrate, as per Eq. (23), that $\Re$ increases with decreasing $D_s=C_s^2A_R^{4/3}$, in Fig. 7(b) different symbols are used according to D_s creating horizontal bands of distinct symbol type consistent with increasing $\Re$. Note that the bands also shift to higher $\mathrm{Re}_{\mathrm{LES}}$ with increasing $\Re$ and $C_s^2A_R^{4/3}$ as per Eqs. (26) and (29).

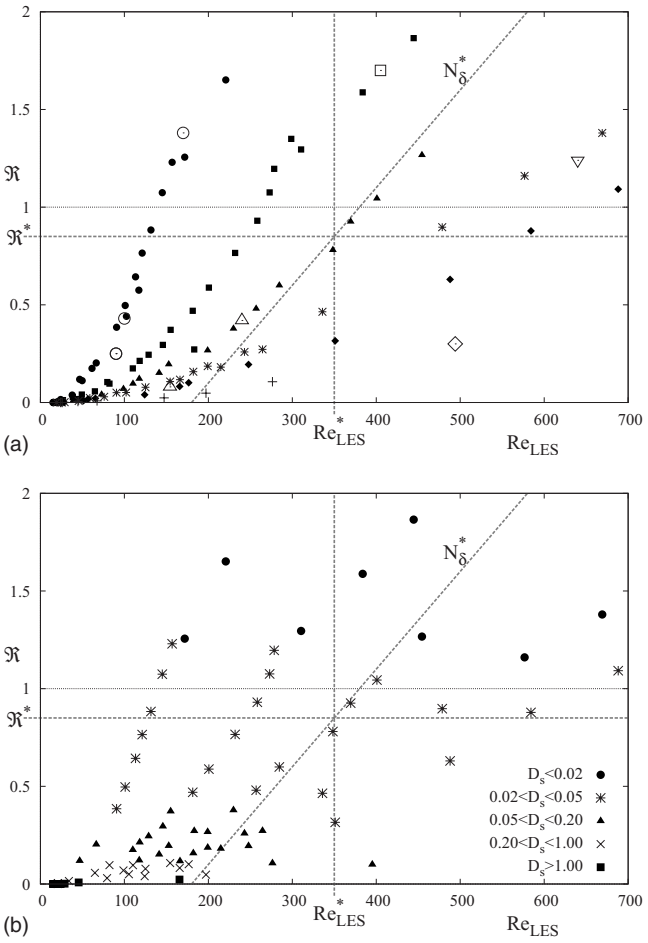

FIG. 7. The simulations carried out for this study shown on the $\Re-\mathrm{Re}_{\mathrm{LES}}$ parameter space. (a) The LES grouped according to N_z, where $N_z=32$ (●), 64 (■), 96 (▲), 128(∗), 160 (♦), and 256(+). Also included are LESs from several previous studies by Andren *et al.* (○) (Ref. 14), Sullivan *et al.* (△) (Ref. 2), Porté-Agel *et al.* (□) (Ref. 4), Chow *et al.* (◇) (Ref. 5), and Drobinski *et al.* (▽) (Ref. 32). (b) The LES grouped according to $D_s=C_s^2A_R^{4/3}$.

B. The high accuracy zone

To show the transition from subcritical regions of the $\Re-\mathrm{Re}_{\mathrm{LES}}$ parameter space to the supercritical HAZ, consider the 16 simulations on the four paths shown in Fig. 8 with the point symbols. Each path has a fixed vertical resolution N_z and progresses from lower to higher $\Re$ and $\mathrm{Re}_{\mathrm{LES}}$ along lines of constant N_z, roughly lines of constant slope $(\xi_2\tilde{\kappa}_1/N_\delta)$ in Eq. (31).

In Fig. 9 we plot $\Phi_m(z)$ against z/δ for each of the groups of four simulations at fixed N_z in Fig. 8. In Sec. IV A we argued for the existence of a critical vertical resolution N^*_δ below which the surface layer is insufficiently resolved and the LOTW can therefore not be properly captured. The four groups of curves in Fig. 9 show the consequences of poor resolution of the surface layer in the vertical and provide an estimate for N^*_δ. In Fig. 9(a) the surface layer is resolved with, at best, three grid points. This clearly insufficient vertical resolution is associated with $\Phi_m(z)$ curves that incorrectly bend to the left from the surface with increasing z; this occurs even when $\Re$ exceeds 1. Furthermore, the underresolution of the surface layer in the vertical affects the mean velocity gradient and mean velocity profiles throughout the boundary layer; the mean gradient decreases too rapidly in z. It is not until Fig. 9(c), $N_z=96$, that this spurious drop in Φ_m with z transitions to the profile $\Phi_m(z)$ extending vertically from the surface as is required by LOTW. The number of grid points in the surface layer (up to $z/\delta=0.2$) is 8–9, suggesting that this is the critical resolution for the surface layer and that N^*_δ for these LESs is ~40–45. We have drawn a line at constant slope $\kappa/N^*_\delta=0.4/45$ in Figs. 7 and 8 showing how paths (a) and (b) remain outside the HAZ and paths (c) and (d) enter the HAZ at higher $\Re$ and $\mathrm{Re}_{\mathrm{LES}}$.

By comparing the groups of Φ_m curves (c) and (d) in Fig. 9, we note that as the simulations progress to higher $\Re$

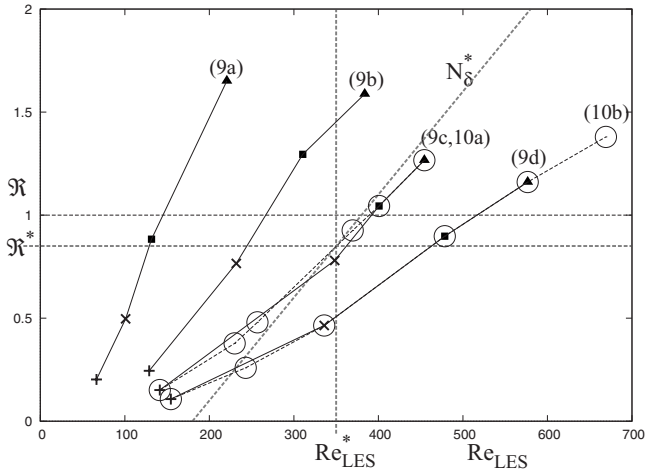

FIG. 8. The systematic variations on the $\Re - Re_{LES}$ parameter space for the simulations plotted in Figs. 9 and 10. Figure 9(a) shows four simulations with the same vertical resolution, $N_z=32$, but decreasing $C_s^2 A_R^{4/3}$ represented by +, ×, ■, and ▲. The vertical resolutions in Figs. 9(b)–9(d) are $N_z=64$, 96, and 128, respectively. The open circles show the locations of the six simulations in Figs. 9(a) and 9(b). The vertical resolutions in Figs. 10(a) and 10(b) are $N_z=96$ and 128, respectively.

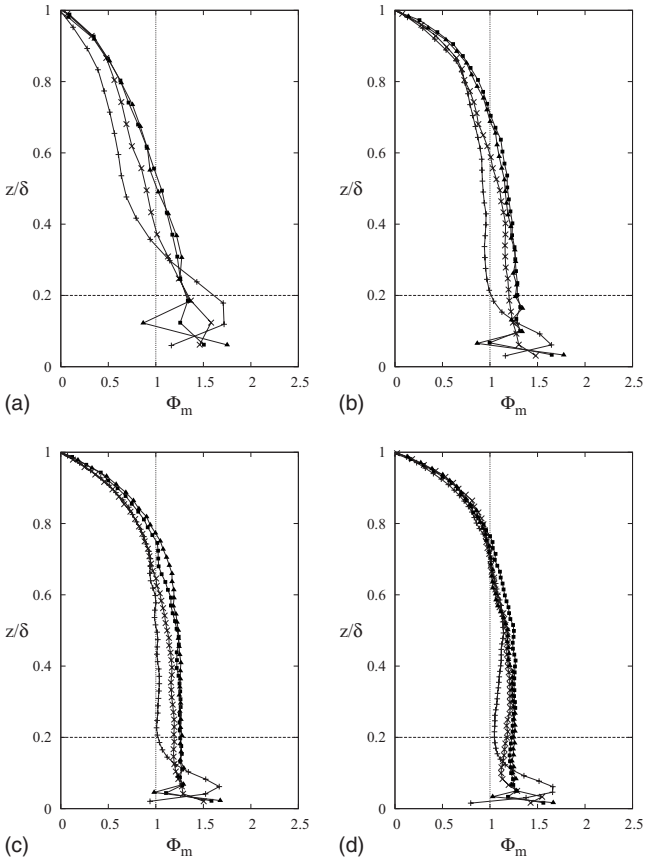

FIG. 9. Effect of vertical grid resolution on the LES predictions of mean shear. Refer to Fig. 8 for the locations of the individual simulations on the $\Re - Re_{LES}$ parameter space. $\Re$ and Re_{LES} progressively increase in each figure in this order: +, ×, ■, ▲. (a) $N_z=32$, $N_x=N_y$ increased from 32(+) to 128 (▲). (b) $N_z=64$, $N_x=N_y$ increased from 64(+) to 240 (▲). (c) $N_z=96$, $N_x=N_y$ increased from 64(+) to 288 (▲). (d) $N_z=128$, $N_x=N_y$ increased from 64(+) to 360 (▲). $\kappa=0.4$ is assumed in forming Φ_m. δ is defined as the height where $\Phi_m=0$. The dashed horizontal lines indicated the upper margin of the surface layer.

and Re_{LES} along lines of constant N_z, in both groups the final two curves approach grid independence and the LOTW is captured as the overshoot is suppressed. To study the transition in the surface layer in detail, and to estimate $\Re^*$ and Re_{LES}^*, we compare the six simulations shown in Fig. 8 with the open circles which lie along each of the two paths, $N_z=96$ and $N_z=128$. The variations in $\Phi_m(z)$ in the lower 40% of the boundary layer for each point along the two paths are shown separately in Fig. 10. Comparing the upper and lower sets of figures, we observe nearly identical transitions along each of the two paths into the HAZ. At the lowest $\Re$ and Re_{LES} an overshoot obscures the surface layer and the LOTW is not predicted by the LES. As $\Re$ and Re_{LES} increase (by decreasing $C_s^2 A_R^{4/3}$), the same transition in $\phi(z)$ takes place along each path: the overshoot progressively decreases and a region of constant $\Phi_m(z)$ progressively strengthens until a well-defined region of constant $\Phi_m(z)$ appears in the surface layer that is maintained when $\Re^*$ and Re_{LES}^* exceed about 0.85 and 350, respectively, using the Smagorinsky closure. (The oscillations near the surface will be discussed in Sec. VII.) The estimates for the lines that define the HAZ from the critical Smagorinsky model parameters $\Re^* \approx 0.85$, $Re_{LES}^* \approx 350$, and $N_\delta^* \approx 45$ are drawn in Figs. 7, 8, and 11(a).

Figure 10 shows that as N_z, C_s, and A_R are adjusted so as to progressively move the LES from the subcritical part of the parameter space into the HAZ, the mean velocity gradient approaches a fixed point independent of the path taken into the HAZ. In Fig. 11 we plot the normalized mean velocity gradient distributions for five of our computed LESs within the HAZ at different vertical grid resolutions N_δ and combinations $C_s^2 A_R^{4/3}$. Figure 11(a) shows the locations of these five simulations on the $\Re - Re_{LES}$ parameter space (all but the + symbol). Figure 11(b) shows that these simulations within the HAZ are approximately grid independent over the boundary layer depth. In Fig. 11(c) we expand the surface layer to show how the overshoot is suppressed and the LOTW is captured by the simulation (all but the dashed line).

In Fig. 7(a) we also show simulations from the literature. All but the simulation by Drobinski *et al.*[32] is well outside the HAZ. In two simulations, one from Andren *et al.*[14] and one from Porté-Agel *et al.*,[4] $\Re$ was sufficiently high to remove the overshoot but the vertical resolution of the grid was insufficient for the LES to produce LOTW scaling.

In Fig. 11(a) the Drobinski *et al.*[32] simulation is indicated with the plus symbol and in Fig. 11(c) with the dashed line. Drobinski *et al.*[32] used a different numerical algorithm and a one-equation eddy viscosity model. Their model for surface shear stress was not indicated. Whereas their critical parameters $\Re^*$ and Re_{LES}^* are not necessarily the same (since they used a different SFS stress closure), their simulation appears to be well within the HAZ [Fig. 11(a)], their overshoot is suppressed and they have captured LOTW scaling [Fig. 11(c)]. The Drobinski *et al.*[32] simulation predicts a different numerical value for $\phi(z)$ in the surface layer than do our simulations with the classical Smagorinsky closure and Moeng[38] surface stress model. Whereas the Smagorinsky

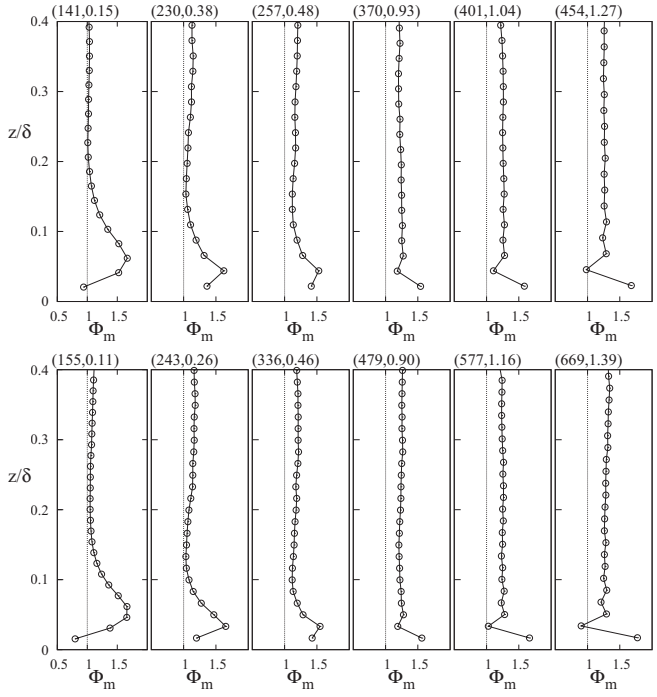

FIG. 10. Change in structure of $\Phi_m(z)$ as the LES moves toward and into the HAZ. Refer to Fig. 8 for the locations of the individual simulations on the $\Re - \mathrm{Re}_{\mathrm{LES}}$ parameter space; $\Re$ and $\mathrm{Re}_{\mathrm{LES}}$ progressively increase in each panel from left to right. Top panel: LES with $N_z=96$. Bottom panel: LES with $N_z=128$. $\mathrm{Re}_{\mathrm{LES}}$ and $\Re$ are given on top of each figure as $(\mathrm{Re}_{\mathrm{LES}},\Re)$. $\kappa=0.4$ is assumed in forming Φ_m. δ is defined as the height where $\Phi_m=0$.

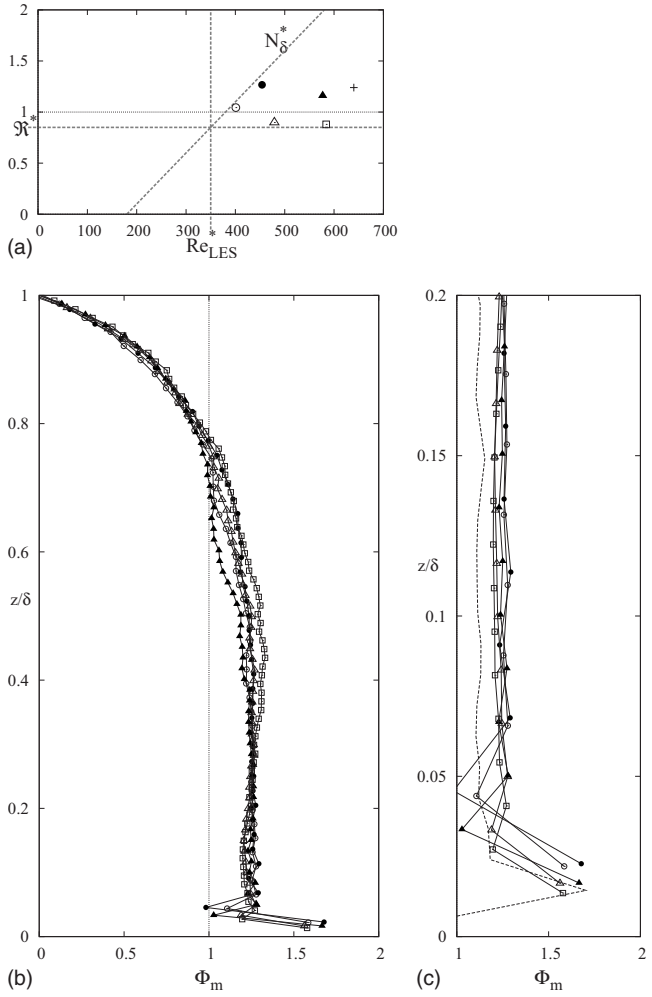

FIG. 11. Five simulations in the HAZ at different N_δ and $D_s \equiv C_s^2 A_R^{4/3}$, demonstrating the convergence of the predictions of $\Phi_m(z)$ to a relatively grid-independent solution without the overshoot and capturing the LOTW. (a) gives the locations of the five simulations in HAZ. $\Phi_m(z)$ from Drobinski *et al.* (Ref. 32) are given in (c) with the dashed curve and in (a) with the plus symbol (+). $\kappa=0.4$ is assumed in forming Φ_m. δ is defined as the height where $\Phi_m=0$.

model simulations in Fig. 11 predicted a von Kármán constant $\kappa \approx 0.33$, the Drobinski *et al.*[32] simulation produces a $\kappa \approx 0.35$. Factors that affect the prediction of the von Kármán constant are discussed in Sec. VII C

It turns out that the von Kármán constant issue is associated with the development of oscillations in $\Phi_m(z)$ at grid cells adjacent to the surface (Fig. 10). The oscillations grow as the simulations move farther into the HAZ along a line of constant N_z. As will be discussed in Sec. VII, the oscillations originate from the spurious nature of the lower boundary condition for fluctuating surface shear stress. This observation is interesting, in part, because it has been previously reported that the LES of the ABL is insensitive to the details of the lower stress boundary condition.[2,41] These simulations, however, were outside the HAZ and in the presence of the overshoot and its frictional source.

VII. DISCUSSION

We consider a LES in which one models only what is required in order to close the numerical problem, where LOTW is a prediction and not a forced result. We restrict the problem to Reynolds numbers where viscous or surface roughness scales cannot be resolved by the grid, which we regard as highly practical. In this scenario, to close the discretized dynamical system, it is necessary to produce a closure for SFS stress and a model for total horizontal stress fluctuations at the surface. Anything beyond this is out of the scope of our analysis.

We have developed a theory to explain the basic issues underlying deviations from LOTW scaling for mean velocity gradient and we laid out a strategy for the design of LES of high Reynolds number wall bounded turbulent flows based on the theoretical arguments. These deviations extend beyond the overshoot in scale mean velocity gradient to encompass LOTW of mean velocity in general. In this section we organize this understanding and briefly refer to new issues that have arisen from this study and we discuss the application of the current framework to the logarithmic layer mismatch problem in hybrid RANS/LES methods such as DES.[18]

A. Breakdown in law-of-the-wall scaling: Interior versus surface

Deviations from the LOTW in mean velocity and velocity gradient in the inertial surface layer arise from a competition between the characteristic velocity length scales u_* and z and other velocity or length scales that enter either from the

true fluid physics or during the conversion to the discretized dynamical system that is ultimately advanced on the computer. Turbulence motions in the surface layer at the characteristic length scale z, for example, may compete with motions at the boundary layer scale (Khanna and Brasseur[21]) or with the influences of surface friction or roughness that are characterized by the length scales $\ell_\nu = \nu/u_*$ and z_0. If sufficiently strong, these confounding scales will alter the scaling $\partial U/\partial z \sim u_*/z$ in the inertial surface layer. LOTW assumes that this is not the case and experiments in the laboratory and atmosphere have generally supported this assumption when there are no confounding scales and the ratio of the outer to viscous length and roughness scales is sufficiently large. However, when the influence of confounding characteristic scales is sufficiently strong to compete with u_* and z in the inertial surface layer, deviations from LOTW result.

What we have shown here is that in the conversion from the exact continuous dynamical system to the LES discretized dynamical system that is actually advanced on the computer, additional characteristic scales are introduced into the simulated dynamics that can interfere with LOTW scaling in the surface layer when sufficiently strong. Several elements in the simulation might introduce spurious characteristic scales: (i) models of existing terms and new terms that are introduced into the governing equation, (ii) models for unknown boundary conditions, (iii) the type and order of the discretization of derivatives together with grid geometry, and (iv) algorithmic additions, for example, to maintain numerical stability. The current study has focused primarily on the influences of a spurious viscous length scale that is introduced within the computational domain by the model for the SFS stress tensor. This spurious scale is a reflection of the manner in which the net transfer of turbulence energy from resolved to SFSs is modeled. Whereas the interscale interactions that underlie the transfer of energy are purely inertial in reality, all practical closures for the SFS stress tensor model the net transfer of energy from the resolved scales by a dissipative mechanism that removes energy at the smallest resolved scales.

However, the SFS stress is often not the only term that is modeled in the conversion from the continuous to the discrete dynamical system. At the very high Reynolds numbers of practical interest, and at which LOTW is valid, the surface viscous layer, if it exists, cannot be resolved in a LES. The vertical derivatives in resolved and SFS stress therefore require that a model be supplied for the total stress at the surface. Hybrid schemes couple a RANS SFS stress model on a very high aspect ratio RANS grid in an extremely thin surface viscous layer with LES and SFS closure on a LES grid beginning in the lower inertial surface layer, also very near the surface. Thus, the LES part of the simulation obtains the lower boundary condition on stress from the RANS part of the simulation, which is far from exact. Nonhybrid schemes must supply a model for the total horizontal shear stress, generally written as a function of resolved velocity within the computational domain. So, in addition to any spurious scales introduced *within* the computational domain by the SFS stress model, there exists the possibility that the model for surface shear stress might introduce spurious scales at the *boundary* of the LES computational domain.

We have found experimentally that standard surface stress models do introduce spurious effects that force deviations from LOTW at the first couple grid levels adjacent to the surface. Figure 10 shows that this additional confounding contribution from the lower stress boundary condition is obscured when the frictional contribution from the interior SFS stress is sufficiently overwhelming to produce the overshoot. When the LES is moved into the HAZ so that the viscous effects causing the overshoot are suppressed, the confounding influences of the surface stress model become apparent and spread vertically as the relative contribution from the interior SFS stress model diminishes with increasing $\mathfrak{R}$. Current research shows that adjustments to surface shear stress are possible which significantly reduce the spurious influence of standard surface stress models.[42]

B. Breakdown in law-of-the-wall scaling in the interior of the computational domain

Interior to the computational domain, deviations from LOTW scaling of mean velocity gradient depend on the strength of the spurious viscous contribution that creates the length scale $\ell_{\nu_{\mathrm{LES}}}$ in competition with z in the surface layer. We find that the strength of $\ell_{\nu_{\mathrm{LES}}}$ relative to z depends on three characteristics of the simulation: the viscous content of the model as determined by the structure of the representation of the SFS stress and the model constant(s), the relative contribution of the resolved inertial stress to the SFS stress in the mean, and the degree of the vertical resolution of the surface layer by the grid. Interestingly, although these three characteristics are interdependent, the relative contribution of inertial to SFS shear stress ($\mathfrak{R}$) is not equivalent to the LES Reynolds number $\mathrm{Re}_{\mathrm{LES}}$, the ratio of outer boundary layer scale to inner (spurious) LES viscous scale, $\delta/\ell_{\nu_{\mathrm{LES}}}$.

With eddy viscosity closures, we find that $\mathfrak{R}$ is inversely proportional to the combination $D_t = C_t^a A_R^{\ b}$, where C_t is the model constant, A_R is the grid aspect ratio, and a, b are model dependent [Eq. (23)]. Since, in the mean, the sum of the resolved and SFS shear stresses is independent of model for stationary channel flow, the ratio $\mathfrak{R}$ can be increased either by reducing the SFS stress (by reducing C_t) or by increasing the relative spectral content of resolved to SFS scales in the horizontal (by reducing A_R). As $\mathfrak{R}$ increases, the LES viscous scale is eventually sufficiently contained within the first grid cell that the LOTW scale z dominates $\ell_{\nu_{\mathrm{LES}}}$ and the overshoot is removed. In Sec. IV B we estimate that $\ell_{\nu_{\mathrm{LES}}}$ must be less than about 20% of the first grid height to remove the influence of $\ell_{\nu_{\mathrm{LES}}}$ sufficiently to eliminate the overshoot on the grid.

However, we also show that removing the overshoot does not necessarily produce a prediction that fully captures LOTW—that is, in which $\phi(z)$ is constant through the surface layer. In the actual flow, LOTW requires the ratio of boundary layer to viscous scale to be large enough that frictional effects are suppressed in the inertial surface layer sufficiently for $\partial U/\partial z$ to scale on u_*/z. Correspondingly, in a LES the spurious LES viscous scale $\ell_{\nu_{\mathrm{LES}}}$ must be sufficiently small relative to the boundary layer scale δ to fully

capture LOTW. Unlike the real flow, however, in the LES $\ell_{\nu_{\mathrm{LES}}}$ must also be sufficiently small relative to the grid scale Δ_z ($\mathfrak{R}>1$) and, as a consequence, the Reynolds number $\mathrm{Re}_{\mathrm{LES}}=\delta/\ell_{\nu_{\mathrm{LES}}}$ depends both on $D_t=C_t^a A_R^{\ b}$ and on N_δ, the vertical resolution of the grid. Thus, although the relative contribution of resolved to SFS stress $\mathfrak{R}$ can be adjusted and the overshoot removed by changing the model constant and the grid aspect ratio in the combination D_t, $\mathrm{Re}_{\mathrm{LES}}$ is dependent also on N_δ: $\mathrm{Re}_{\mathrm{LES}}$ decreases with decreasing vertical grid resolution, to the point that at the exceptionally poor resolution given by the thin solid line in Fig. 5(c), the simulation is effectively laminar. More relevant, however, when $\mathfrak{R}>\mathfrak{R}^*$ but the surface layer is poorly resolved in the vertical ($\mathrm{Re}_{\mathrm{LES}}<\mathrm{Re}^*_{\mathrm{LES}}$), the overshoot is gone but $\phi(z)$ is not constant in the surface layer. As a result, the prediction for mean velocity is not grid independent throughout the boundary layer [Figs. 9(a) and 9(b)].

Based on the above discussion, we have designed a parameter space from Eq. (31) in which the SFS model parameters can be adjusted in combination with grid aspect ratio and vertical grid resolution to systematically move the LES into the supercritical region of the parameter space $\mathfrak{R}>\mathfrak{R}^*$, $\mathrm{Re}>\mathrm{Re}^*_{\mathrm{LES}}$, and $N_\delta>N^*_\delta$ that we call the high accuracy zone (HAZ). The LES must reside within the HAZ for the spurious scales within the computational domain to be suppressed sufficiently and for the grid vertical resolution to be high enough for the simulation to capture LOTW in mean velocity. However, in principle, the spurious LES viscous scale $\ell_{\nu_{\mathrm{LES}}}$ will also strengthen in the presence of numerical dissipation, which is dependent on the discretization scheme or is sometimes added algorithmically in a regularization procedure. In the numerical experiments discussed here, we applied a minimally dissipative spectral code. The extent to which more dissipative discretization schemes enhance the spurious viscous influences and deviations form LOTW scaling has yet to be explored.

In Sec. III D the eddy viscosity closure was written in the general form $\nu_t=\ell_t u_t$ and in the scaling analysis and numerical experiments we have taken $\ell_t=C_t\tilde{\ell}_t=C_t\Delta$ constant. However in some closures ℓ_t is modeled as a function of z, either by specifying $\tilde{\ell}_t=\tilde{\ell}_t(z)$ or by allowing $C_t=C_t(z)$ to vary with z through a dynamic procedure. In the latter case, the relationships involving $D_t=C_t^a A_R^{\ b}$ should use $C_t(z_1)$, the value of C_t at the first grid level. In the former case, when $\tilde{\ell}_t(z)$ is a specified function of z, C_t should be replaced with $\tilde{\ell}_t(z_1)/\Delta$.

C. Elements in LES prediction of the von Kármán constant

Interestingly, Fig. 10 also shows that when the overshoot exists ($\mathfrak{R}<\mathfrak{R}^*$) with good vertical grid resolution ($N_\delta>N^*_\delta$), $\Phi_m(z)$ can go roughly constant *above* the surface layer at a value that would be consistent with a von Kármán constant of ≈ 0.40 if the constant $\Phi_m(z)$ region had been in the surface layer rather than above it. On the other hand, the LES of Fig. 5 has similar physics to the channel flow DNS of Fig. 3, since both show increasing Reynolds number in the presence of a friction-induced overshoot (Re_τ with real overshoots in Fig. 3 versus $\mathrm{Re}_{\mathrm{LES}}$ with spurious overshoot in Fig. 5). Although the respective Reynolds numbers in these figures are too low to expect full LOTW scaling in the inertial surface layer, the trend in each case is a shift to higher Φ_m with increasing Reynolds number. When both $\mathrm{Re}_{\mathrm{LES}}$ and $\mathfrak{R}$ are increased to move the LES into the HAZ so that $\Phi_m(z)$ goes constant in the surface layer in Fig. 11, Φ_m shifts to even higher values and the von Kármán constant is found to converge to ≈ 0.33.

Although the classical Smagorinsky closure for SFS stress was used in our numerical experiments, we have produced similar results with a one-equation eddy viscosity model[38] and a two-equation noneddy viscosity based model.[43] Many of these simulations produce von Kármán constants closer to 0.35, similar to the prediction by Drobinski *et al.*[32] in Fig. 11, which was obtained with a one-equation SFS stress model (and an unknown wall stress model). However, we also find that when the simulations in Fig. 10 are redone using a modified surface shear stress model,[42] the $\Phi_m(z)$ curves in Fig. 11 shift to the left and the predicted von Kármán constant increases to ≈ 0.35. Thus, both the SFS stress closure and surface stress models can affect the prediction of κ.

According to our theory, $\mathfrak{R}$ and $\mathrm{Re}_{\mathrm{LES}}$ depend on model constant C_t and aspect ratio A_R always in the combination $D_t=C_t^a A_R^{\ b}$, where a and b are model dependent. However, there must exist lower and upper bounds on C_t and A_R individually. For example, it would be untenable to maintain the simulation in the HAZ with D_t fixed but with C_t and A_R close to the limits $C_t\to 0$ and $A_R\to\infty$; this limit would produce a RANS simulation with zero SFS stress. Similarly, allowing $C_t\to\infty$ and $A_R\to 0$ in the LES with fixed D_t is equally untenable. It is clear that bounds must exist on C_t and A_R, and therefore there must also exist bounds on D_t, $\mathfrak{R}$, $\mathrm{Re}_{\mathrm{LES}}$, and the upper margin of the HAZ of Fig. 6. Interestingly, it turns out that the von Kármán constant depends weakly on C_t and A_R within practical bounds and systematic adjustment leads to $\kappa\approx 0.37$.

A predicted von Kármán constant in the range of 0.35–0.37 for the ABL is not inconsistent with estimates from the data collected in the field. As discussed in Sec. I, although the values for the von Kármán constant obtained from experiment are not yet definitive, it seems clear that κ is not universal. Like the ratio between energy flux from the large scales and dissipation rate at the small scales in high Reynolds number turbulence,[44] the ratio between $\partial U/\partial z$ and u_*/z in the surface layer of the high Reynolds number boundary layer appears to depend on outer scale characteristics of the flow such as pressure gradient and flow geometry.[6] Nagib and Chauhan[6] present the most recent estimates for κ from ≈ 0.37 in channel flow to ≈ 0.41 in pipe flow. Although a von Kármán constant as low as 0.33 has been reported for the neutral ABL,[8] $\kappa\sim 0.35$–0.37 is commonly reported.[10–13] A recent compilation by Andreas *et al.*[7] estimates κ to be ≈ 0.387 in the range of roughness Reynolds numbers $z_0^+\sim 2$–100.

If the value for κ does depend on the details of the outer flow as proposed, it would not be surprising to find that the

proportionality constant between $\partial U/\partial z$ and u_*/z in LES with LOTW scaling depends on simulation parameters that influence the predicted large-eddy structure of the flow. We find that modifications to the surface stress model that suppress the unphysical oscillations at the surface (Fig. 10) also influence the characteristics of the flow that underlie the predicted von Kármán constant.

D. Application to the logarithmic layer mismatch

It was pointed out in Sec. II B and shown in Fig. 2 that the phenomenon that we have described as an overshoot has been identified as a logarithmic layer mismatch or superbuffer layer in DES.[17–19] (Based on the current paper, the term superbuffer layer is more accurately a "superviscous layer.")

Figure 2(b) shows that the logarithmic layer mismatch, or DES overshoot, occurs within the inertial surface layer of the simulation on a LES grid with $A_R \sim O(1)$. Below this region the grid aspect ratio becomes very high and the simulation transitions to RANS in the viscous sublayer of this smooth wall channel flow. In context with the $\Re - \mathrm{Re}_{\mathrm{LES}}$ parameter space methodology developed in this paper, the lower margin of the LES grid will start in the lower portion of the inertial surface layer, roughly $z^+ \sim 100$. Relative to this LES grid, the model for surface stress is replaced by the stress predicted within the transition regions between the RANS and LES grids. The key point is that the LES part of the hybrid simulation sees a grid at the lower margin of the inertial surface layer with an "effective grid cell" between the lower margin of the LES grid at $z^+ \sim 100$ and the surface. In our theory, then, A_R would be the aspect ratio of this effective grid cell and C_t would be the model constant used in the LES closure for SFS stress. The constants a and b in $D_t = C_t^a A_R^{\ b}$ will depend on the type of SFS stress closure applied in the hybrid formulation. Then, using Fig. 6, Eq. (31), and the procedure outlined in Sec. V with the effective grid cell, it should be possible to remove the logarithmic layer mismatch and adjust the simulation to capture LOTW in $\partial U/\partial z$, albeit potentially with residual interference from the RANS part of the simulation near the surface.

E. Comments on the role of the SFS stress closure

What we have presented in this study are essential requirements for any SFS stress closure necessary to produce proper scaling for mean velocity in the surface layer in a LES that does not apply external mechanisms that force the existence of a logarithmic profile in mean velocity. All current practical SFS closures use friction to remove energy from the resolved scales as a replacement for what is, in reality, a fully inertial transfer of turbulent kinetic energy from resolved to SFS motions. The methods we present here are particularly relevant to the design of LES using such models.

One might ask if it is theoretically possible to develop a closure for SFS stress (or SFS stress divergence) that is fully inertial. There are theoretical arguments that suggest that such models may be possible in principle.[45] A few such models do exist;[29,46,47] however, in practice these are found to require the addition of a viscous component.[47,48] A closure with no dissipative physics would imply infinite $\Re$ and $\mathrm{Re}_{\mathrm{LES}}$, independent of the grid. The current study suggests that one cannot dissociate the design of the grid (aspect ratio and vertical resolution) from the design of the closure (model constant, characteristic length, and velocity scales) to create a LES that properly predicts LOTW scaling in mean velocity.

Whereas we argue that the basic theory and the requirements we have developed herein are relevant to all wall-bounded LES that does not explicitly force the existence of LOTW, we do not imply that all SFS closures are equal. For example, we have pointed out that the critical parameters $\Re^*$, $\mathrm{Re}^*_{\mathrm{LES}}$, and N^*_δ are closure dependent, and that details of the closures for SFS and surface stress affect the predicted value of the von Kármán constant. In addition, however, one can anticipate a significant dependence between the structure of the closure and the space-time details of predicted turbulence statistics, spectra, and scale-dependent dynamics, especially in nonstationary, nonequilibrium, and complex wall-bounded turbulent flows. The theory and framework developed in this study will be useful for future advancements of SFS modeling specific to the surface layer in LES of wall-bounded turbulent flows.

ACKNOWLEDGMENTS

We are grateful to the Army Research Office for financial support of this research and to our program monitor Walter D. Bach, Jr. for his personal interest and insights. We also gratefully acknowledge the assistance with the code from Dr. Martin Otte, Dr. Yong Zhou, and Dr. Mark Kelly, and insightful discussions with Dr. Peter Sullivan and Dr. Chin-Hoh Moeng at the National Center for Atmospheric Research, Dr. Philippe Spalart at Boeing Commercial Airplanes, Mr. Sanjiv Ramachandran at Penn State University, and Dr. Robert Moser at University of Texas Austin. Finally, we thank Dr. Drobinski for providing data from their LES (Ref. 32) to plot $\Phi_m(z)$ in Fig. 11(c).

APPENDIX A: MODIFICATIONS OF EQUATIONS WHEN THE CORIOLIS FORCE IS ACTIVE

As pointed out in Sec. III D, when the Coriolis force is present, as in LES of the ABL, the velocity at the first grid level is at an angle θ_1 to the geostrophic wind velocity above the boundary layer. In this case, Eqs. (19)–(21), (23), (28), and (29) contain an additional factor $\xi_3 \equiv \cos\theta_1$. For completeness, we write the equations here with ξ_3 inserted in the correct places,

$$\langle s_{13}^r \rangle_1 = \left(\frac{\partial U}{\partial z} \right)_1 \equiv \frac{\xi_3 u_*}{\tilde{\kappa}_1 z_1}, \tag{A1}$$

$$\nu_{\mathrm{LES}} = \frac{\xi_1 \xi_3}{\beta} D_t u_* \Delta_z \quad \text{(eddy viscosity)}, \tag{A2}$$

$$\Re = \frac{T_{\mathrm{tot}_1}}{T_{S_1}} - 1 = \frac{\xi_2 \xi_3 (\rho u_*^2)}{T_{S_1}} - 1 \quad \text{(closure independent)}, \tag{A3}$$

$$\Re = \frac{\xi\beta\tilde{\kappa}_1}{D_t} - 1, \quad \text{where} \quad \xi = \frac{\xi_2}{\xi_1\xi_3} \quad \text{(eddy viscosity)}, \tag{A4}$$

$$T_{S_1} = 2\rho\nu_{\text{LES}}\langle s_{13}^r\rangle_1 = \rho\nu_{\text{LES}}\frac{\xi_3 u_*}{\tilde{\kappa}_1 z_1} \quad \text{(closure independent)}, \tag{A5}$$

$$\ell_{\nu_{\text{LES}}} \equiv \frac{\nu_{\text{LES}}}{u_*} = \frac{\xi_1\xi_3}{\beta}D_t\Delta_z \quad \text{(eddy viscosity)}, \tag{A6}$$

$$\text{Re}_{\text{LES}} = \frac{\beta}{\xi_1\xi_3}\frac{N_\delta}{D_t} \quad \text{(eddy viscosity)}. \tag{A7}$$

For the Smagorinsky model $\beta=\tilde{\kappa}_1$ and $D_t=C_s^2 A_R^{4/3}$. For the one-equation model β is an order one constant and $D_t=C_k A_R^{8/9}$.

APPENDIX B: DETAILS OF THE LARGE-EDDY SIMULATIONS

The pseudospectral LES code used in this study follows a line of evolution that began with the code of Moeng[38] and Sullivan *et al.*[40] The version we used evolved from a parallel version of the Sullivan code by Otte.[49] We only give a brief review of the algorithm; more details of the algorithm are in Moeng[38] and Sullivan *et al.*[40] Because the simulated ABL is homogeneous in the horizontal directions, a mixed scheme of spectral in the horizontal directions and second-order accurate central finite differencing in the vertical is used. A uniform staggered mesh is used in the vertical direction; the first vertical velocity plane (w) is at a distance of Δ_z from the surface, and the first horizontal velocity (u,v) plane is at $\Delta_z/2$ from the surface. A nonstaggered mesh is used in the horizontal directions, and horizontal derivatives are computed in spectral space. Dealiasing is carried out in the homogeneous horizontal directions by padding with the 2/3 rule. As previously mentioned, all values of grid size and aspect ratio in this paper and the Smagorinsky length scale are based on the grid before padding by 3/2 in both horizontal directions.

The LES equations were solved in a computational domain of $3000\ \text{m}\times 3000\ \text{m}\times 1000\ \text{m}$ with uniformly spaced grid points. The geostrophic wind was set to $(U_g,V_g)=(15\ \text{m/s},0)$ and the surface heat flux was set to zero. The initial velocities were uniform except for small random fluctuations added to the lowest four grid levels. To maintain a quasistationary boundary layer in the long time limit, a capping inversion temperature profile was defined in the upper half of the computational domain and the temperature equation was calculated with a Boussinesq buoyancy term in the momentum equation. Below the capping inversion the temperature was maintained constant so buoyancy forces were zero within the boundary layer itself. The time integration uses an explicit third-order accurate multistage Runge–Kutta scheme (RK3) with a variable time step.[40] A CFL number of 0.25 was typically used at each stage (or CFL=0.75 for an entire step).

The horizontally averaged (mean) velocity in the center of the boundary layer was plotted in time in all simulations to determine when the transient evolution period has passed and statistics could be reliability obtained. Even in the long-time limit, however, buoyancy force within the capping inversion region produces a temporally oscillating mean velocity at longer times. In this study we gathered statistics roughly after about 15 large-eddy turnover times (z_i/u_*) and were careful to collect statistics for several eddy turnover times always at the same temporal phase in the oscillation. Even with this care, some statistical variability can be observed in mean shear in the outer boundary layer in Fig. 11(b).

Periodic boundary conditions were applied in the horizontal directions. The geostrophic wind components were specified on the upper margin of the computational domain well outside the turbulent boundary layer. In order to evaluate the vertical derivative in SFS stress, it is necessary to provide a model for the total fluctuating shear stress at the surface. We have used both the nonlinear model described in Moeng[38] and the linear model of Schumann;[50] there are only minor differences in the mean velocity predictions. We present here only the results with the nonlinear model. With this model, the total surface shear stress is specified as proportional to the square of the horizontal velocity at the first grid level.

Roughness is modeled only in the sense that increasing roughness moves the surface layer farther from the surface increasing the surface drag. To this end, we specify the ratio of mean wind at the first grid level to the friction velocity u_*, $R_U \equiv |\langle \mathbf{u}^r\rangle|_1/u_*$ in terms of a roughness height z_0, and the friction velocity is determined at each time step by dividing the predicted mean wind at the first grid level with R_U. It should be noted that, as is typical, the ratio R_U is parametrized in terms of z_0 using a LOTW formula for the mean wind. However, it is important to recognize that this parametrization of R_U in terms of z_0 does not force the simulation to satisfy the law-of-the-wall anywhere, including the first grid level. For all simulations in the current study, $z_0=16$ cm and $z_0/\Delta_z \ll 1$.

[1] P. J. Mason and D. J. Thomson, "Stochastic backscatter in large-eddy simulations of boundary layers," J. Fluid Mech. **242**, 51 (1992).
[2] P. P. Sullivan, J. C. McWilliams, and C.-H. Moeng, "A subgrid-scale model for large eddy simulation of planetary boundary-layer flows," Boundary-Layer Meteorol. **71**, 247 (1994).
[3] B. Kosovic, "Subgrid-scale modeling for the large-eddy simulation of high-Reynolds-number boundary layers," J. Fluid Mech. **336**, 151 (1997).
[4] F. Porté-Agel, C. Meneveau, and M. B. Parlange, "A scale-dependent dynamic model for large-eddy simulation: Application to a neutral atmospheric boundary layer," J. Fluid Mech. **415**, 261 (2000).
[5] F. K. Chow, R. Street, M. Xue, and J. H. Ferziger, "Explicit filtering and reconstruction turbulence modeling for large-eddy simulation of neutral boundary layer flow," J. Atmos. Sci. **62**, 2058 (2005).
[6] H. M. Nagib and K. A. Chauhan, "Variations of von Kármán coefficient in canonical flows," Phys. Fluids **20**, 101518 (2008).
[7] E. L. Andreas, K. L. Claffey, R. E. Jordan, C. W. Fairall, P. S. Guest, P. O. G. Persson, and A. A. Grachev, "Evaluation of the von Kármán constant in the atmospheric surface layer," J. Fluid Mech. **559**, 117 (2006).
[8] R. J. Francey and J. R. Garratt, "Interpretation of flux-profile observations at ITCE (1976)," J. Appl. Meteorol. **20**, 603 (1981).
[9] U. Högström, "Review of some basic characteristics of the atmospheric surface layer," Boundary-Layer Meteorol. **78**, 215 (1996).

[10]J. A. Businger, J. C. Wyngaard, Y. Izumi, and E. F. Bradley, "Flux-profile relationships in the atmospheric surface layer," J. Atmos. Sci. **28**, 181 (1971).
[11]J. C. Wyngaard, J. A. Businger, J. C. Kaimal, and S. E. Larsen, "Comments on 'A revaluation of the Kansas mast influence on measurements of stress and cup anemometer overspeeding'," Boundary-Layer Meteorol. **22**, 245 (1982).
[12]J. W. Telford and J. A. Businger, "Comment on von Kármán's constant in atmospheric boundary layer flow: Reevaluated," J. Atmos. Sci. **43**, 2127 (1986).
[13]S. P. Oncley, C. A. Friehe, J. C. Larue, J. A. Businger, E. C. Itsweire, and S. S. Chang, "Surface-layer fluxes, profiles, and turbulence measurements over uniform terrain under near-neutral conditions," J. Atmos. Sci. **53**, 1029 (1996).
[14]A. Andren, A. R. Brown, J. Graf, P. J. Mason, C.-H. Moeng, F. T. M. Nieuwstadt, and U. Schumann, "Large-eddy simulation of a neutrally stratified boundary layer: A comparison of four computer codes," Q. J. R. Meteorol. Soc. **120**, 1457 (1994).
[15]J. C. Wyngaard, "Toward numerical modeling in the 'Terra Incognita'," J. Atmos. Sci. **61**, 1816 (2004).
[16]P. R. Spalart, W. H. Jou, M. Strelets, and S. R. Allmaras, "Comments on the feasibility of LES for wings and on a hybrid RANS/LES approach," in *Advances in DNS/LES*, edited by C. Liu and Z. Liu (Greyden, Columbus, OH, 1997), Vol. 137.
[17]N. V. Nikitin, F. Nicoud, B. Wasistho, K. D. Squires, and P. R. Spalart, "An approach to wall modeling in large-eddy simulation," Phys. Fluids **12**, 1629 (2000).
[18]P. R. Spalart, "Detached-eddy simulation," Annu. Rev. Fluid Mech. **41**, 181 (2009).
[19]U. Piomelli and E. Balaras, "Wall-layer models for large-eddy simulations," Annu. Rev. Fluid Mech. **34**, 349 (2002).
[20]S. Khanna and J. G. Brasseur, "Three-dimensional buoyancy- and shear-induced local structure of the atmospheric boundary layer," J. Atmos. Sci. **55**, 710 (1998).
[21]S. Khanna and J. G. Brasseur, "Analysis of Monin-Obukhov similarity from large-eddy simulation," J. Fluid Mech. **345**, 251 (1997).
[22]M. A. LeMone, "The structure and dynamics of horizontal roll vortices in the planetary boundary layer," J. Atmos. Sci. **30**, 1077 (1973).
[23]N. Hutchins and I. Marusic, "Evidence of very long meandering structures in the logarithmic region of turbulent boundary layers," J. Fluid Mech. **579**, 1 (2007).
[24]A. Juneja and J. G. Brasseur, "Characteristics of subgrid-resolved-scale dynamics in anisotropic turbulence, with application to rough-wall boundary layers," Phys. Fluids **11**, 3054 (1999).
[25]F. Ding, S. P. Arya, and Y.-L. Lin, "Large-eddy simulation of the atmospheric boundary layer using a new subgrid-scale model," Environ. Fluid Mech. **1**, 29 (2001).
[26]E. Lévêque, F. Toschi, L. Shao, and J.-P. Bertoglio, "Shear-improved Smagorinsky model for large-eddy simulation of wall-bounded turbulent flows," J. Fluid Mech. **570**, 491 (2007).
[27]I. Esau, "Simulation of Ekman boundary layers by large eddy model with dynamic mixed subfilter closure," Environ. Fluid Mech. **4**, 273 (2004).
[28]V. C. Wong and D. K. Lilly, "A comparison of two dynamic subgrid closure methods for turbulent thermal-convection," Phys. Fluids **6**, 1016 (1994).
[29]Y. Zhou, J. G. Brasseur, and A. Juneja, "A resolvable subfilter-scale model specific to large-eddy simulation of under-resolved turbulence," Phys. Fluids **13**, 2602 (2001).
[30]S. Stolz, N. A. Adams, and L. Kleiser, "The approximate deconvolution model for large-eddy simulations of incompressible flows," Phys. Fluids **13**, 997 (2001).
[31]A. R. Brown, J. M. Hobson, and N. Wood, "Large-eddy simulation of neutral turbulent flow over rough sinusoidal ridges," Boundary-Layer Meteorol. **98**, 411 (2001).
[32]P. Drobinski, P. Carlotti, J.-L. Redelsperger, R. M. Banta, V. Masson, and R. K. Newsom, "Numerical and experimental investigation of the neutral atmospheric surface layer," J. Atmos. Sci. **64**, 137 (2007).
[33]P. R. Spalart, private communication (2008).
[34]P. J. Mason, "Large-eddy simulation: A critical review of the technique," Q. J. R. Meteorol. Soc. **120**, 1 (1994).
[35]K. Iwamoto, Y. Suzuki, and N. Kasagi, "Reynolds number effect on wall turbulence: Toward effective feedback control," Int. J. Heat Fluid Flow **23**, 678 (2002).
[36]K. Iwamoto, "Database of fully developed channel flow," THTLAB Internal Report No. ILR-0201, THTLAB, Department of Mechanical Engineering, The University of Tokyo, 2002.
[37]S. Hoyas and J. Jimenez, "Scaling of the velocity fluctuations in turbulent channels up to Re_τ=2003," Phys. Fluids **18**, 011702 (2006).
[38]C.-H. Moeng, "A large-eddy-simulation model for the study of planetary boundary layer turbulence," J. Atmos. Sci. **41**, 2052 (1984).
[39]G. K. Batchelor, *The Theory of Homogeneous Turbulence* (Cambridge University Press, Cambridge, England, 1953).
[40]P. P. Sullivan, J. C. McWilliams, and C.-H. Moeng, "A grid nesting method for large-eddy simulation of planetary boundary-layer flows," Boundary-Layer Meteorol. **80**, 167 (1996).
[41]J. C. Wyngaard, L. J. Peltier, and S. Khanna, "LES in the surface layer: Surface fluxes, scaling, and SGS modeling," J. Atmos. Sci. **55**, 1733 (1998).
[42]J. G. Brasseur, T. Wei, and S. Ramachandran, "Predicting law-of-the-wall with LES: Role of SFS and surface stress models," Bull. Am. Phys. Soc. **54**, 228 (2009).
[43]S. C. Hatlee and J. C. Wyngaard, "Improved subfilter-scale models from the HATS field data," J. Atmos. Sci. **64**, 1694 (2007).
[44]K. R. Sreenivasan, "An update on the energy dissipation rate in isotropic turbulence," Phys. Fluids **10**, 528 (1998).
[45]R. D. Moser, N. P. Malaya, H. Chang, P. S. Zandonade, P. Vedula, A. Bhattacharya, and A. Haselbacher, "Theoretically based optimal large-eddy simulation," Phys. Fluids **21**, 105104-1 (2009).
[46]J. Bardina, J. H. Ferziger, and W. C. Reynolds, "Improved subgrid-scale models for large-eddy simulation," AIAA Pap. **80**, 1357 (1980).
[47]C. Meneveau and J. Katz, "Scale-invariance and turbulence models for large-eddy simulation," Annu. Rev. Fluid Mech. **32**, 1 (2000).
[48]J. G. Brasseur and Y. Zhou, "A resolvable subfilter-scale model specific to large-eddy simulation of near-wall turbulence," Bull. Am. Phys. Soc. **45**, 82 (2000).
[49]M. J. Otte, "Turbulent structure of the interfacial layer capping the atmospheric boundary layer," Ph.D. thesis, Department of Meteorology, The Pennsylvania State University, 2002.
[50]U. Schumann, "Subgrid-scale model for finite difference simulation of turbulent flows in plane channels and annuli," J. Comput. Phys. **18**, 376 (1975).